Multiple crustal and mantle inputs in post-collisional magmatism: Evidence from late-Variscan Sàrrabus pluton (SE Sardinia, Italy)

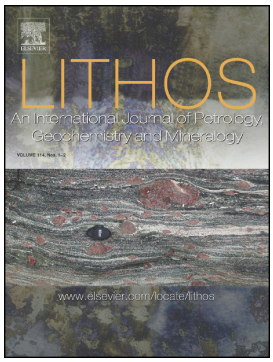

Multiple crustal and mantle inputs in post-collisional magmatism: Evidence from late-Variscan Sàrrabus pluton (SE Sardinia, Italy)

F. Secchi, T. Giovanardi, S. Naitza, M. Casalini, M. Kohút, A.M. Conte, G. Oggiano

PII: S0024-4937(22)00106-2

DOI: https://doi.org/10.1016/j.lithos.2022.106697

Reference: LITHOS 106697

To appear in: *LITHOS*

Received date: 20 October 2021

Revised date: 31 March 2022

Accepted date: 31 March 2022

Please cite this article as: F. Secchi, T. Giovanardi, S. Naitza, et al., Multiple crustal and mantle inputs in post-collisional magmatism: Evidence from late-Variscan Sàrrabus pluton (SE Sardinia, Italy), *LITHOS* (2021), https://doi.org/10.1016/j.lithos.2022.106697

Multiple crustal and mantle inputs in post-collisional magmatism: evidence from late-Variscan Sàrrabus pluton (SE Sardinia, Italy)

Secchi, F[1,2], Giovanardi, T[3,*] tommaso.giovanardi@unimore.it**, Naitza, S[4], Casalini, M[5], Kohút, M[6], Conte A.M[7], Oggiano G**[1]

[1]Dipartimento Chimica e Farmacia, Via Piandanna 4, I-07100 Sassari (Italy). Università degli Studi di Sassari, Sassari (Italy).
[2]CNR-Istituto di Geologia Ambientale e Geoingegneria, Sede Secondaria di Cagliari, Via Marengo 2, 09123 Cagliari, Italy.
[3]Dipartimento Scienze Chimiche e Geologiche, Via G. Campi 103, I-41125 Modena. Università degli Studi di Modena e Reggio Emilia, Modena (Italy).
[4]Dipartimento Scienze Chimiche e Geologiche, Cittadella Universitaria S. S. 554 bivio per Sestu, I-09042 Monserrato (CA). Università degli Studi di Cagliari, Cagliari (Italy).
[5]Dipartimento Scienze della Terra, Via LA Pira 4, I-50121 Firenze. Università degli Studi di Firenze, Firenze (Italy)
[6]Earth Science Institute, Slovak Academy of Sciences, Dúbravská cesta 9, 840 05 Bratislava, Slovakia.
[7]CNR-IGAG, Sede di Roma, c/o DST Sapienza Università di Roma, P.le Aldo Moro 5, I-00185, Roma, Italy.
[*]Corresponding author.

Abstract

The Sàrrabus pluton is formed by multiple short-lived intrusions emplaced at about 286 Ma at shallow crustal levels within the external part of the South Variscan Orogenic Belt. A chemical and Sr and Nd isotopic study on the Variscan post-collisional magmatism from the Sàrrabus pluton reveals the repeated bimodal character of the intrusions, in which heterogeneous crustal sources and mantle-derived calcalkaline magmas are involved. Products of this magmatic activity occur as intrusive units and mafic/felsic dykes intruded in post-collisional regime along extensional faults during tectonic exhumation. Pluton growth started with an early stage of emplacement of broadly granodioritic magma with subordinate mafic magma batches (stage 1) followed by large intrusions of metaluminous to subaluminous and subordinately peraluminous granites (stage 2). In stage 1, the occurrence of remnants of stratified olivine-bearing gabbroic rocks indicates the intrusion of mafic magmas which experienced low-pressure crystal/liquid fractionation. Mafic magmas may represent an external heat supply for melting of different crustal materials belonging to an inferred Precambrian crystalline basement underlying the Paleozoic rocks of the Variscan nappe pile. Strong evidence for heterogeneous crustal sources is constrained by isotope data. Peraluminous granites and felsic dikes display initial $^{87}Sr/^{86}Sr$ in the range of 0.7140÷0.7215 and a roughly constant εNd_{286} (–7.4 to –7.5). Conversely, a peculiar less radiogenic character, in the range of 0.7030÷0.7067/–5.5÷–6.2, is observed for metaluminous to subaluminous varieties. Calculated Neodymium Crustal Index (NCI) confirmed a progressive increase in crustal magmas generation during the pluton growth, from stage 1, recording minor mixing processes between mantle- and crustal-derived peraluminous melts, to stage 2, where extensive crustal melting occurred, originating metaluminous to subaluminous granites. Possible crustal sources for metaluminous/subaluminous and peraluminous granites are (Pan-African) amphibolites and metasedimentary rocks, respectively. Two-stage depleted-mantle Nd model ages cluster at 1.4 and 1.6 Ga for metaluminous/subaluminous and peraluminous granites, respectively, well comparable with other

segments of the European Variscan belt. Remarkably, last magmatic pulses resulted in widespread subalkaline bimodal mafic/felsic dykes that overlapped the Sr–Nd signature recorded by major intrusions. This similar geochemical affinity between late dykes and the first intrusives may be related to decreasing temperature in the crust, which inhibited extensive mixing processes with the upwelling melts. At the same time, the presence of felsic intrusions in the shallow crust would have prevented the rise of more primitive basic magmas, which would have consolidated at depth. Finally, the high radiogenic character of Sàrrabus mafic products, compared to coeval Variscan mafic rocks of Corsica and northern Sardinia, may be indicative of previous fractionation and mixing processes, possibly related to magmatic underplating of the lower crust.

Keywords: (Late-Variscan magmatism, bimodal magmatism, dilatant shear zones, crustal sources, Sr-Nd isotopes, Neodymium crustal index)

Introduction

The Corsica-Sardinia Batholith (CSB) belongs to the southern Variscan belt of Europe and represents a key area for studies on post-collisional evolution of this orogenic chain (Ferrè and Leake, 2001; Paquette et al., 2003; Cocherie et al., 2005; Rossi et al., 2009, 2015; Edel et al., 2014; Casini et al., 2015a, b; Conte et al., 2017) (Fig. 1). The CSB was emplaced through a complex succession of discontinuous short-lived tectonic and magmatic episodes from the late collisional stages to the post-collisional collapse and exhumation of the orogenic roots. At present, a general agreement exists in literature in considering the control of lithospheric shear zones on the emplacement of major intrusive complexes of the CSB (Edel et al., 2014; Casini et al., 2012; 2015; Cuccuru et al., 2016), and the involvement of metaigneous and metasedimentary crustal sources with subordinate mantle contribution (Poli et al., 1989; Cocherie et al., 1994; Tommasini et al., 1995; Macera et al., 2011; Rossi et al., 2015; Conte et al., 2017). Also, the heat source necessary to generate the large volumes of crustal-derived intrusive magma in the post-collisional regime of SCB was related to lithospheric delamination and asthenospheric upwelling promoting partial melting of lower crust (Gaggero et al., 2007; Rossi et al., 2015). As a result, a wide range of crustal melts and hybrid varieties, mainly of broadly granodioritic composition, produced by mafic/felsic magma interactions, contributed to the architecture of the entire batholith. Common effect of mafic/felsic magma interaction was documented by igneous dark enclaves dispersed in granodiorites and subordinately in monzogranites (Poli et al., 1989; Zorpi et al., 1991; Barbey et al., 2008; Casini et al., 2015b). Mantle-derived magmas, commonly intruding in the final stages of the CSB growth, are represented by gabbroic magma batches and mafic dikes. The tholeiitic and calcalkaline mafic dikes spread over the whole batholith, and partly within the host metamorphic basement. Even if recent radiometric ages point to a substantial contemporaneity among the main

intrusive events and the subalkaline mafic dike swarms (Rossi et al., 2015; Conte et al., 2017), the genetic linkage between this hypabyssal activity and the plutons making the batholith was never taken into consideration.

The Sàrrabus pluton (south-eastern Sardinia), is formed by multiple intrusions emplaced within the shallow crustal levels of a fold and thrust belt along the Gondwana foreland; it shows peculiar characteristics compared to the rest of the CSB due to the different geochemical affinities of the magma intrusions and their coeval ages. Previous studies performed on the Sàrrabus pluton (Brotzu et al., 1981, 1993; Poli and Tommasini, 1999; Ronca et al., 1999; Conte et al., 2017; Franciosi et al., 2019) focused on single aspects of the pluton without proposing a global genetic model. In a recent study, Secchi et al. (2021) firstly recognized the substantial contemporaneity of a wide spectrum of magma pulses concentrated in a short time span, forming a relatively small pluton (400 km^2), which differentiate the Sàrrabus pluton with respect to others in CSB.

In this work, field evidence and chemical and isotopic data (Sr and Nd bulk rock and Hf in zircons) are presented and discussed with data from previous studies, to constrain the petrogenesis of the entire Sàrrabus pluton. We will focus on the nature of involved crustal sources which originated the granitic units of the pluton and their interactions with mantle derived melts. We will propose a genetic model of growth of the Sàrrabus pluton by magma ascending through lithospheric-scale shear zones active in an extensional post-collisional setting which could be applied to other shallow crustal magmatic complexes rooted on lithospheric shear zones.

Geological setting

The Variscan orogenic wedge

The Variscan collisional frame of Sardinia and Corsica results in a high-grade, inner, anatectic complex retaining remnants of eclogite and high-pressure mafic granulite well exposed in Corsica and northern Sardinia (Cruciani et al., 2015), which overthrusts a complex pile of nappes showing low- to medium- grade metamorphic imprint (Fig. 1). The nappe pile in turn overrides, with general top- to- southwest transport, a non-metamorphic foreland located in southern Sardinia (Carmignani et al., 1994), which is commonly interpreted as a Gondwana foreland (Edel et al., 2014; Rossi et al., 2015 and reference therein). This frame is the result of the early Carboniferous collision between the northern Gondwana margin, and the ribbon-like collage of terranes interposed between Gondwana and Laurussia after the (present time) north-directed subduction of an oceanic domain, namely the Paleo-Tethys or South-Armorican Ocean (Stampfli et al., 2003; Oggiano et al., 2010; Gaggero et al., 2012). The Variscan crust was thus highly heterogeneous, consisting of several

assembled terranes and syn-collisional plutonic intrusions. During the post-collisional evolution of the chain, the Variscan crust was widely reworked in the general context of a strike slip dextral mega shear zone (Casini and Funedda, 2014; Rossi et al., 2015; Edel et al., 2016). This reworking was coeval with the collapse (Ruben Diez and Preira, 2016) of the previously thickened crust and by heating related to slab breakoff of the north-directed subducting oceanic lithosphere as well as to shear heating (Casini et al., 2012). This post collisional frame in Sardinia, similarly to the entire Variscides, went on with *HT*/*LP* metamorphism (Kröner and Willner, 1998; Casini and Oggiano, 2008) and was accompanied by intensive magmatic activity giving rise to the CSB. The magmatic activity is coeval with lithospheric-scale shear zones and anatexis in the 320÷305 Ma wide interval, as well as to extension and to the clockwise rotation of Corsica-Sardinia microplate (Rossi et al., 2009, 2015; Edel et al., 2014).

The Corsica-Sardinia Batholith

The CSB resulted from the succession of discrete, short-lived plutonic and volcanic events of broadly calcalkaline affinity, which may be grouped into three main magmatic peaks based on geographic, geochronological and magmatic criteria as follows:

(1) late-collisional magmatic peak, only documented in western and northwestern Corsica within a short time span of 344 ÷ 335 Ma (Cocherie et al., 2005);

(2) older post-collisional magmatic peak (hereafter OMP, *sensu* Conte et al., 2017), poorly represented in southern Sardinia lasting from 322 ± 8 Ma (northern Sardinia; Casini et al., 2015a) to 299 ± 3 Ma (central Sardinia; Meloni et al., 2017);

(3) younger post-collisional magmatic peak (hereafter YMP, *sensu* Conte et al., 2017) widespread in Sardinia and Corsica and referred to the short time span of 291÷286 Ma (Cocherie et al., 2005; Casini et al., 2015a).

The igneous activity belonging to the syn-collisional peak resulted in a rock-association made up of quartz monzonites to syenogranites with enclaves of ultrapotassic mafic rocks (the so-called Mg-K rock-suite; Cocherie et al., 1994 and reference therein), emplaced from deep crustal levels up to shallow conditions.

The architecture of CSB is instead closely related to the post-collisional stages of the Variscan orogen. With the exception of the earlier andalusite-bearing foliated granodiorites and leucogranites occurring in northernmost of Sardinia (i.e., Barrabisa and Santa Maria Island: 321 ± 8 ÷ 313 ± 6 Ma; Oggiano et al., 2007; Casini et al., 2012), the OMP is characterized by repeated sequences of monzogranitic and granodioritic pulses with subordinate mafic rocks, which represent the dominant intrusive activity in the internal nappe zone of northern-central Sardinia. Overall, magma pulses emplaced almost constantly at shallow crustal levels (about 2–4 kbar; Casini et al., 2012; Conte et

al., 2017; Bosi et al., 2019). Shallow conditions are constrained by the common development of narrow contact aureoles with andalusite-cordierite hornfelses around the plutons, as well as by geobarometric results (Conte et al., 2017; Bosi et al., 2019 and reference therein); in addition, andalusite and cordierite may occur as fundamental phases in peraluminous varieties (e.g., Barrabisa and Gennargentu, Fig. 1; Casini et al., 2012; Gaeta et al., 2013).

In the external nappe zone and in the Gondwanan foreland of southern Sardinia, the OMP is only represented by small plutons with inverse zonation belonging to an ilmenite rock-*series* and ranging from granodiorites to peraluminous cordierite-bearing granites (e.g., Arbus and Grighini) with local small amounts of olivine-bearing monzo-gabbronorites (Arbus, Capo Pecora and Burcèi) (Secchi et al., 1991; Brotzu et al., 1993; Musumeci et al., 2014) (Fig. 1).

The intrusive bodies belonging to YMP are dominated by voluminous (mainly NE-trending) peraluminous to subaluminous felsic and minor mafic intrusions emplaced at the shallowest crustal levels (about 1 kbar; Gaggero et al., 2007; Conte et al., 2017 and reference therein). Granodioritic sequences associated to mafic bodies cover a restricted time span of 286 ± 1 ÷ 279 ± 1 Ma (Paquette et al., 2003; Casini et al., 2015a). The age of these late intrusions overlaps that of peralkaline granites which are only exposed in northern Corsica (Cocherie et al., 2005). In southern Sardinia, metaluminous to sub-aluminous granites are dominant over peraluminous granites. They mainly belong to ilmenite rock-*series* and show a F-rich ferroan character as well as a peculiar metallogenic signature as testified by Sn-W-Mo and F ores (Naitza et al., 2017).

Exposed rock-types are dominantly felsic (over 90% granodiorites and granites), with only minor amounts of gabbroic rocks commonly associated with tonalites mingled with host granodiorites (Zorpi et al., 1991). The production of magmas in the CSB is largely interpreted as related to contemporaneous partial melting of crustal materials and interactions of felsic melts with mafic magmas at several levels in the crust (Secchi et al., 1991; Zorpi et al., 1991; Tommasini and Poli 1992; Cocherie et al., 1994; Tommasini et al., 1995; Di Vincenzo et al. 1996; Poli and Tommasini, 1999; Renna et al., 2006; Barbey et al., 2008). According to Rossi et al. (2015), the voluminous felsic activity marking the end of YMP in the entire CSB reflects a phase of intense crustal heating triggered by lithospheric delamination and intrusion of mafic magmas in the lower crust. Heating contribution in this phase has also been related to intense shearing (Casini et al., 2012; 2015b) and radiogenic heating (Puccini et al., 2013).

The 291÷286 Ma emplacement age interval identified for YMP overlaps with U/Pb data determined for *HT-LP* granulites from the Variscan deep crust exhumed along the “European” margin of the thinned Tethys margin from Corsica and Calabria, which are in the range of 285÷280 Ma (Rossi et al., 2015).

Furthermore, the early Permian intrusive magmatism is coeval with calcalkaline felsic/intermediate volcanism associated to the onset of continental basins in an extensional/transtensional regime (Cortesogno et al., 1998; Gaggero et al., 2017).

Based on SHRIMP analyses on zircons, the late calcalkaline mafic dykes from Corsica provided age values of 279 ± 1 Ma (Cocherie et al., 2005).

The Sàrrabus pluton

The Sàrrabus pluton -exposed for over 400 km^2- is formed by multiple, short-lived pulses emplaced at shallow crustal levels within an anchi-metamorphosed Cambro-Ordovician volcano-sedimentary sequence in the frontal part of the orogenic wedge of the SE Sardinia (Fig. 1). Its original extension and shape are unknown, as the contact with the host rocks is limited to its northern boundary (Fig. 2) even if small roof pendants of metamorphic basement are locally exposed along the southern Sardinian coastline. The pluton may be framed in a dilatant extensional/transtensional shear zone bordering the Sardinia-Corsica tectonic microplate to the E (Secchi et al., 2021). It consists of different generations of granodiorites, associated to gabbroic rocks and tonalites, and of metaluminous, subaluminous and subordinately peraluminous granites, all referable to the YMP. The pluton shows abundant mafic and felsic dikes crosscutting the main intrusions, thus representing the later igneous activities.

The available geochronological data support a restricted time interval of emplacement for the whole pluton, with ages clustered around 286 Ma (Secchi et al., 2021). In detail, U/Pb data on single zircons yielded overlapping ages at 287 ± 1 Ma for the S. Vito leucogranite satellite intrusion (Dack, 2009) and at 286 ± 9 Ma for the Cala Regina granodiorites (Secchi et al., 2021). These ages are in good agreement with Ar-Ar and Rb/Sr data available for S. Vito leucogranite and Cala Regina granodiorites yielding 285 ± 1 and 292 ± 17 Ma, respectively (Dini et al., 2005; Secchi et al., 2021).

The geology of the pluton has been recently outlined by Secchi et al. (2021; Fig.2). The intrusive sequence may be schematized as follows. The older part of Sàrrabus pluton (hereafter the *stage 1*) is an intrusive sequence of EW/ENE trending pulses of granodiorites and coeval mafic batches, well exposed along the southern Sardinian coastline (Fig. 2). The granodioritic pulses have been defined by Secchi et al. (2021) as Cala Regina, Monte Cresia and Monte Nai units; in this study they are hereafter reported together as the Cala Regina Group. In the field, size and abundance of microgranular dark enclaves and frequency of mafic bodies in granodiorite increase from N to S. In their southernmost outcrops, where they are intruded by the NE trending, peraluminous granite of Monte Maria-Unit, granodiorites contain in addition hololeucocratic felsic enclaves (Fig. 3a).

The Cala Regina Group granodiorites locally grade into foliated quartz-diorite and tonalite with highly stretched hybrid enclaves (Fig. 3b), dismembered syn-plutonic dikes and decametric bodies of elongated two pyroxene-bearing hornblende-gabbroic rocks with local remnants of olivine-bearing layers (i.e., cumulitic rocks of Solànas Complex; SO in Fig. 2). The magmatic foliation trends roughly E-W and is sub-vertical or steeply dipping to the south. It is defined by the preferred orientation of dark mica, feldspar and stretched microgranular mafic enclaves. The magmatic lineation, where observed, plunges down dip and is defined mostly by alignment of dark mica, feldspars as well as the long axis of mafic enclaves (Fig. 3b). Close to the coast, along a 2 km wide belt roughly trending E-W, extremely stretched enclaves occur in large proportion along banded mafic-felsic domains (Fig. 3c), these features have been related to mingling processes (Poli and Tommasini 1989) enhanced by a normal, syn-plutonic shear zone, namely the South Sarrabus Shear zone (SSSZ; Secchi et al 2021; Fig. 2). The coeval intrusion of mafic and felsic magmas favored localized magma mixing, which resulted in the local production of heterogeneous magmas of broadly tonalitic composition. This magma emplaced by lateral expansion in a NS direction that is common to the other pulses (Secchi et al., 2021).

The younger part of Sàrrabus pluton is dominated by a group of at least three different pulses of F-rich ferroan granites (hereafter as *stage 2*), which intrude the granodiorites and range from biotite granites (Bruncu Nicola Bove Unit and San Priamo Unit) to hastingsite granites (Monte Sette Fratelli Unit). The first two granitic intrusions were emplaced along an E-W trend while the Monte Sette Fratelli Unit overlaps the others emplaced as a large sub-vertical stock. Contacts of the three are parallel to the contact of stage 1 Monte Cresia unit with the surrounding Paleozoic metasediments.

This general frame is complicated by the occurrence of a bimodal subalkaline rock-association made up of a several generations of NNW trending mafic and (metaluminous to subaluminous) felsic dykes crosscutting an earlier generation of NE trending peraluminous felsic dikes dated at 293 ± 3 Ma (Ronca et al., 1999; Fig. 3*e*; *f*). Remarkably, mafic dikes consist of spessartites to hornblende-bearing granular rocks and is prevalently outcropping in Cala Regina Group granodiorites exposed in southern portion of the pluton. The end of Sàrrabus igneous activity is represented by a generation of olivine plagioclase-phyric mafic dikes with tholeiitic signature (Ronca et al., 1999) that crosscuts granite intrusions with a dominant NS trend.

Analytical methods

Whole-rock major and trace element concentrations of twelve samples representing the different Sàrrabus lithologies were determined at Activation Laboratories, Ancaster, Ontario, Canada.

Powdered samples were previously fused using lithium metaborate or tetraborate, and then rapidly digested in weak nitric acid solutions. Resulting solutions were analyzed by inductively coupled plasma–optical emission spectroscopy (ICP–OES) and ICP–mass spectrometry (ICP–MS) techniques. The uncertainties in major element concentrations are generally between 1% and 3%, except for MnO (5%–10%) and P_2O_5 (>10%); most trace elements concentrations have uncertainties of <5%. Major element concentrations usually have detection limits of 0.01 wt%. Loss on ignition (L.O.I.) and FeO contents were measured using standards gravimetric techniques and titration with 10N $KMnO_4$ techniques, respectively. Data are reported in Supplementary Material Table 1.

Additional samples were analysed for major and trace elements by *XRF* spectrometry using powder pellets, at the University of Cagliari laboratories, Italy. *X*-ray analyses were performed on an automatic Philips spectrometer (PW1400). Data were corrected for drift and background effects. Major elements were reduced for matrix effects according to Franzini et al. (1972). Trace elements were reduced for matrix effects using the method of fundamental parameters according to Criss and Birks (1968). Thirty reference rock standards were used for calibration. Analytical accuracy is within ±1% for SiO_2, TiO_2, Al_2O_3, Fe_2O_3, CaO, K_2O and MnO, and ± 4% for MgO, Na_2O and P_2O_5. The accuracy of trace element analyses is ± 2 to 3% at 1000 ppm, ± 5 to 10% at 100 ppm, and ± 10 to 20% at 10 ppm level. Rh and W *X*-ray tubes were used, and detection limits were around 3 ppm for most trace elements. Data are reported in Supplementary Material Table 2.

Eleven selected samples, representing all the Sàrrabus lithologies were analyzed for Sr and Nd isotopic compositions at the laboratories of Dipartimento Scienze della Terra (Università degli Studi di Firenze, Italy). Sr and Nd measurements were obtained by a Thermofisher Triton Plus multi-collector mass-spectrometer, running in a static mode, following separation of Sr and Nd using conventional ion-exchange procedures as reported in Avanzinelli et al. (2005). Measured $^{87}Sr/^{86}Sr$ ratios were normalized to $^{88}Sr/^{86}Sr = 8.375209$, $^{143}Nd/^{144}Nd$ ratios to $^{146}Nd/^{144}Nd = 0.7219$. During collection of isotopic data, replicate analyses of the Sr NIST SRM 987 ($SrCO_3$) isotopic standards gave an average $^{87}Sr/^{86}Sr$ value of 0.710251 ± 20 ($2\sigma_m$, N = 100) well in agreement with the reference value of Thirwall, (1991). The in-house Nd isotopic standard NdFi (Nd oxide) was used to test reproducibility. Data are reported in Supplementary Material Table 3.

Lu-Hf analyses were performed on the same zircon crystals previously U-Pb dated by Secchi et al. (2021) on SSP2 sample from Cala Regina granodiorite (Capo Carbonara, Fig. 2). Analyses were done in the same dated domains and were carried out using a double focusing MC–ICP-MS with a forward Nier–Johnson geometry (Thermo Fisher Scientific, Neptune™), coupled to a 213 nm Nd:YAG laser ablation system (New Wave Research™) at the laboratory of Centro Interdipartimentale Grandi Strumenti of the Università di Modena e Reggio Emilia. Isotopic ratios

were acquired in static mode with a block of 250 cycles (including laser warm-up, ~50–80 cycles of analysis and washout), an integration time of 0.5 s, a laser spot of 55 μm and a fluence of ~10 J/cm2. A low laser frequency (~10 Hz) was used to achieve better signal stability with a He flux of ~0.5 L/min. Details of the method are reported in Giovanardi et al. (2018). Data reduction was performed using the Hf-INATOR software (Giovanardi and Lugli, 2017). During the analytical session, reference material zircon TEMORA-2 was used to check accuracy and precision. TEMORA-2 provides $^{176}Hf/^{177}Hf$ ratios of 0.282686 ± 0.000075 (2σ, *n*=6), identical within error to the reference value of 0.282686 (Woodhead and Hergt, 2005). Data are reported in Supplementary Material Table 4.

Results

Representative samples from the intrusive units of Sàrrabus pluton have been analyzed for major, trace elements and Sr and Nd systematics to integrate whole-rock data available in the literature for gabbroic rocks and granodiorites (Poli and Tommasini, 1999; Franciosi et al., 2019), granitic units (Conte et al., 2017), as well as for mafic and acidic dikes (Ronca et al., 1999).

Overall, this expanded dataset supports a new and broader petrological and evolutionary picture of the pluton.

According to Miller (1985), in this paper granites with ASI > 1 (ASI = (mol. Al/(Ca+Na+K-1.67*P)<1.0) coupled with the occurrence of a more aluminous mineral phase than dark mica will be classified as peraluminous.

Essential petrographic features

The main petrographic and mineralogical features of Sàrrabus igneous units are outlined in Conte et al. (2017; 2018*a*; *b* and reference therein) and summarized in Fig. 4 and Tab. 1. Rocks were classified according to IUGS's recommendations, using modal compositions obtained by mass balance calculations (Stormer and Nicholls, 1978). In this paragraph we will briefly describe the principal features of the different lithotypes, summarizing information from D'Angelo (1998), Poli and Tommasini (1999), Conte et al. (2017) and Franciosi et al. (2019).

Petrographic differences observed in the Cala Regina granodiorites mainly consist of an increase southward in (*a*) size and amount of dark enclaves, which compositionally range from tonalites to hornblende quartz-gabbros, (*b*) color index (from 14% to 20%), as well as (*c*) abundance of primary Fe-hornblende (1%-4%; $Mg\#_{0.40-0.36}$), respectively. Typical plagioclase feldspar is a light-coloured, slightly zoned andesine (An_{45-41}), even if patchy zoned plagioclases with relic of calcic cores (An_{63-39}; Fig. 4*f*) are locally observed especially in biotite granodiorites. Common accessory phases are

well-developed euhedral allanite, associated with mafic minerals, zircon, monazite, and minor apatite + ilmenite as inclusion on brownish dark mica.

Dismembered mafic masses in granodiorites (Solanas Complex of Cala Regina Group granodiorites) are hornblende gabbroic rocks with relics of ortho- and clinopyroxene, grading to hornblende quartz gabbros. These latter represent the typical composition of dark enclaves (Fig. 4a), and usually show panidiomorphic and fluidal textures characterized by calcic plagioclase (An_{84-45}) with cotectic relationships with Fe-hornblende ($Mg\#_{0.55-0.48}$), dark mica ($Mg\#_{0.48-0.45}$) and interstitial quartz (Fig. 4b). The mafic masses also include olivine-bearing gabbronorites and leuco-gabbros with cumulate textures (Conte et al., 2018*b*; Secchi et al., 2021), which document a dismembered formerly stratified sequence. Cumulitic rocks show commonly poikilitic textures; the dominant mineral assemblage is homogeneous olivine (Fo_{74}) with peritectic relationships with orthopyroxene ($Wo_2En_{77}Fs_{21}$) followed by calcic plagioclase (An_{89-92}) and clinopyroxene ($Wo_{47-42}En_{45-49}Fs_{8-9}$) set in a dominant mass of amphibole of pargasitic composition (Fig. 4c).

Strong petrographic variations are observed within felsic rock-types in terms of mafic mineralogy, feldspar composition as well as typical accessory phases. In detail, granites at the core of Sàrrabus pluton (i.e., Bruncu Nicola Bove Unit - BNB in Fig. 2) range from biotite monzogranite to leucogranite with normal oligo-albitic plagioclase (An_{30-15}). Conversely, the San Priamo granite is made up of coarse-grained pinkish biotite leucogranite showing a slightly less sodic plagioclase feldspar (An_{40-26}), large allanite grains and magnetite as typical accessory phases; additional interstitial dark or, less frequently, white micas are often observed (Fig. 4*g*).

The Monte Maria granite is a garnet-bearing ($Alm_{65-69}Sp_{22-27}Py_5Gr_3$) two-mica variety, locally containing altered cordierite (Fig. 4h), whereas the Monte Sette Fratelli Unit consist of leucogranite grading to monzogranite containing oligo-albitic plagioclase (An_{20-15}), large euhedral Fe-hastingsite and red-brown dark micas as early crystallized phases. Main accessory phases are large allanite + magnetite + ilmenite, mostly included in amphiboles, abundant zircons included in quartz and K-feldspars and anhedral fluorite grains as interstitial phases. In these rocks, dark mica of annitic composition, also occurs as interstitial phase, or as discontinuous coronas on interstitial and altered fayalite grains (Conte et al., 2017).

Main petrographic information on mafic and felsic rocks in dike swarms is outlined by Ronca et al. (1999). Overall, dike swarms recorded similar features observed for compositionally-equivalent intrusive rocks. Generally, the NE trending peraluminous felsic dikes, which predate the other dike swarms, resemble the Monte Maria peraluminous granites: they are characterized by oligo-albitic plagioclase and perthitic orthoclase with minor amounts of dark and white mica and/or spessartine-rich garnet. Remarkably, rare corroded andalusite with continuous coronas of white mica are

occasionally observed. Apatite, zircon, monazite, magnetite and locally tourmaline are the typical accessory phases.

Mafic dikes include rocks of dominant basaltic andesite to andesite composition, with minor amounts of basalts. Overall, an orthopyroxene + clinopyroxene succession replaced by amphibole, is frequently observed in the spessartitic mafic dikes (Fig. 4*d*); when observed, olivine occurs as completely altered phenocrysts. Locally basaltic rock-types display glomero-porphyritic which may be evidence of cumulitic character.

The final generation of basaltic dikes (tholeiitic basalt *sensu* Ronca et al., 1999) are commonly characterized by labradoritic plagioclase feldspar, altered olivine and augite set in a fine-grained matrix of augite, plagioclase, and minor amount of amphibole.

Whole rock chemistry

Major and trace-element chemical compositions of selected samples are reported in Supplementary material Tables 1 and 2. Supplementary material Table 1 reports ICP-MS data for 9 specimens from main intrusive units and 3 representative samples from mafic dikes emplaced in granodiorites. Supplementary Material Table 2 refers to additional unpublished *XRF* data while Supplementary Material Table 5 reports average *XRF* analyses of intrusive units calculated on both our analyses and literature data (Pirinu 1994, D'Angelo. 1998).

Gabbroic and mafic dikes rocks have medium-K character while medium- to high-K character is observed for quartz-gabbroic varieties (Fig. 5*a*). Gabbroic rocks and analyzed mafic dikes (Supplementary Material Table 1) may be defined as high alumina basalts (Fig. 5*b*) and show in addition the prevalence of Na_2O over K_2O as a common feature: Na_2O/K_2O ratio decreases from 2.45 to 1.48 in olivine-bearing gabbros to quartz-gabbros, respectively, and from 2.95 to 1.90 in mafic dikes. In addition, gabbroic rocks show an abrupt increase of FeO/(FeO + MgO) and Na_2O + K_2O – CaO (modified alkali index) with SiO_2 from olivine-bearing gabbroic rocks to quartz gabbroic varieties (Fig. 5*d*).

Conversely, granodiorites and granites are plotted at the end of a high-K rock-*series* (Fig. 5*a*) and show a general increase of peraluminous character with SiO_2 evidenced by ASI in the range of 0.73 ÷ 0.98 (in granodiorites) with a higher value of 1.05 in garnet-bearing granite (Supplementary Material Table 1). A prevalence of K with respect to Na is displayed in granodiorites and garnet-bearing granite in the restricted range of 0.72 ÷ 0.74 and 0.61, respectively (Supplementary Material Tables 1 and 5). In the Frost's and Frost (2001) discrimination diagrams, granodiorites display a magnesian/calc-alkalic signature while granites straddle along the ferroan/alkali-calcic fields (Fig. 5*c*; *d*).

REE normalized contents of different rock-*lithotypes* show a similar LREE enriched pattern and are poorly fractionated in MREE and HREE (Supplementary Material Table 1; Fig. 6). However, some differences could be noticed. Rocks from gabbroic association show a slight decrease of the Eu negative anomalies from two pyroxene-bearing gabbros (Eu/Eu* 0.79 ÷ 0.81) to quartz gabbros (Eu/Eu* 0.63 ÷ 0.74, Supplementary Material Figure 1). Quartz gabbros and two-pyroxenes gabbros display less LREE fractionation (La_N/Sm_N (1.42 ÷ 2.00 in quartz gabbros and 1.6-2.2 in two pyroxene bearing-gabbros) with respect to other gabbroic rocks (Fig. 6). Generally, a direct correlation is found between the Eu anomaly and the La_N/Yb_N ratio, while this latter is inversely correlated to the Gd_N/Yb_N (Supplementary Material Figure 1). Cumulate rocks show Eu/Eu* values around 1 and La_N/Sm_N in the range of 1.9 ÷ 2.9.

Trace elements normalized patterns for gabbroic rocks show negative anomalies for Nb, Ta, P, Ti and Sr and enrichments in more incompatible elements (i.e. Rb, Ba, Th and U; Fig. 7a).

Granodioritic rocks show fractionated LREE (La_N/Sm_N between 2.90 and 4.33) and higher La_N/Yb_N (between 8.02 and 13.53) than mafic rocks, with slightly more pronounced Eu anomalies (Eu/Eu* average of 0.67) (Fig. 6b). In addition, trace elements show depletion for Nb, Ta, Sr and P, and high fractionation for the more incompatible elements (Rb, Ba, Th and U), along with peaks in Sr (Fig. 7b).

Granitic rocks display fractionated LREE, relatively flat HREE patterns with Gd_N/Yb_N values range from 0.95 to 1.45 (Supplementary Material Table 1). Eu/Eu* decrease from 0.33 in Monte Sette Fratelli and San Priamo metaluminous/subaluminous granites to 0.18 in Monte Maria Unit peraluminous granite (Fig. 6b). In detail, granites from Monte Sette Fratelli Unit are more enriched in REE and show a slight fractionation in HREE. Conversely, granites from San Priamo Unit are less enriched in REE and show a convex pattern for M-HREE (Fig. 6d). The picture is complicated by the peraluminous granite (Monte Maria), which shows fractionated enrichment for LREE from La to Nd and almost flat trend from Sm to Lu (except for the Eu negative anomaly), showing LREE contents lower than other granites but HREE almost comparable with those observed for Monte Sette Fratelli granites (Fig. 6d). It is also the only lithology displaying Ba depletion while it also shows Nb, Sr and P negative anomalies (Fig. 7b).

Mafic dykes (basalts to andesite-basalt in composition) show fractionated REE patterns with LREE enrichments (La_N/Yb_N between 5.94 and 8.35) and weak or none Eu anomaly (Eu/Eu* between 1.05 and 0.83). Trace elements are depleted in Nb, Ta and P, and the more primitive dykes have a positive Sr anomaly which became negative in the more evolved ones (Fig. 7a).

With respect to the studied samples, the late felsic dykes show the most heterogeneous REE contents (Fig. 6d). Different REE compositions, which basically overlap both metaluminous and peraluminous granites, point out to several different sources of the parent melts.

Isotope data

Sr and Nd isotopic ratios (Supplementary Material Table 3) have been calculated back to 286 Ma the likely age for intrusive rocks and mafic to felsic dykes (Secchi et al., 2021) assuming a substantially rapid emplacement of magmatic pulses based on the field evidence on the intrusion sequence, as well as on geochronological data.

When schematizing the Sàrrabus pluton as composed by an older *stage 1* and by a younger *stage 2*, the isotope composition may be discussed as follows.

Granodiorites and associated gabbroic rocks show no correlation between 1/Nd and $^{143}Nd/^{144}Nd$ initial values (Supplementary Material Figure 2), as well as between SiO_2 and $^{87}Sr/^{86}Sr_t$ and $\varepsilon Nd_{(t)}$ (not shown). In addition, in the $^{87}Sr/^{86}Sr_t$ vs. $\varepsilon Nd_{(t)}$ diagram (Fig. 8) granodiorites plot in a restricted field, ranging from 0.7088 to 0.7097 and from –5.5 to –6.3, respectively. Remarkably, gabbroic rocks commonly show more radiogenic values for Nd and range in composition from 0.7081/–5.9 to 0.7099/–6.8; overall, a similar behavior is observed in the 1000/Sr vs. $^{87}Sr/^{86}Sr_t$ diagram (Supplementary Material Figure 2). A partial overlap in isotopic data between these groups of rocks is represented by tonalites, confirming field observations of mingling relationships with gabbroic rocks.

In the Rb-Sr and Nd-Sm isochron plot (Supplementary Material Figure 3), only the granodioritic rocks and microgranular quartz-gabbros cluster on a 286 Ma reference line (according to published Pb/Pb chronological data: Secchi et al., 2021), whereas gabbroic rocks show scattered values.

Peraluminous granites belonging to Monte Maria and peraluminous rhyolitic dikes show constant $\varepsilon Nd_{(t)}$ (–7.5) and extremely high $^{87}Sr/^{86}Sr_t$ in the range of 0.7154÷0.724, respectively, which approach to a supracrustal endmember.

Metaluminous to subaluminous granite rock-types belonging to *stage 2* (i.e., Monte Sette Fratelli and San Priamo), which occupy the northern side of the pluton, form an independent group showing a flat trend in the Sr–Nd diagram (barred symbols in Fig. 8; Conte et al., 2017). They exhibit a wide Sr isotopic composition, from 0.703 to 0.7095 and, conversely, a quite homogeneous $\varepsilon Nd_{(t)}$ value of about –7.5 that does not differ from the field of metaluminous felsic dikes reported in Ronca et al. (1999).

In general, in the $^{87}Sr/^{86}Sr_t$ vs. $\varepsilon Nd_{(t)}$ diagram (Fig. 8), mafic dikes overlap the trend described by the entire *stage 1* ranging from 0.7068/–2.9 to 0.7097/–6.2. Is to be noticed that lesser and roughly constant radiogenic compositions (0.7053/–1.35) are recorded for late mafic (tholeiitic) dikes hosted in leucogranites.

Further petrogenetic information may be provided by the Nd crustal residence ages for granites and basaltic dikes, on account of a crustal origin proposed in literature (Ronca et al., 1999; Conte et

al., 2017) and of mafic/felsic magma interactions described in the previous geological section, respectively. Given the observed linear correlation between Sm/Nd and two-stage Nd crustal residence age, a two-stage model is here preferred. Overall, calculated model ages are in the 1.4 – 1.6 Ga range reported for European Variscan chain (Janoušek et al., 1995; Downes et al., 1997; Villaseca et al., 1998). In detail, two-stage Nd crustal residence ages calculated for basaltic dikes are in the range of 1.25 – 1.61 Ga and decrease to 1.11 in olivin-phyric tholeiitic basalts. Metaluminous/subaluminous granites and dikes are in the range of 1.44 ÷ 1.50 Ga; higher values clustered to 1.59 Ga have been obtained for peraluminous granites and dikes.

On the granodiorite sample dated by U-Pb zircon ages by Secchi et al. (2021), Lu-Hf analyses on dated zircons were performed (Supplementary Material Table 4 and Figure 4). $^{176}Hf/^{177}Hf$ ratios for Cala Regina granodiorite (sample SPP2) are between 0.282441 and 0.282621. $\varepsilon Hf_{(t)}$ recalculated back at 286 Ma (Secchi et al. 2021) provided negative values, between -5.6 and -1.0, but a single positive value was also found at 0.5.

Discussion

Geological constraints for Sàrrabus magmatism

The emplacement of Sàrrabus pluton occurred in a crustal segment likely made up of an ancient (Proterozoic) basement belonging to northern Gondwana margin overthrusted by Paleozoic nappes dominated by Cambro-Ordovician anchimetamorphic sedimentary rocks (Carmignani et al., 1994; Edel et al., 2014).

Field (Secchi et al., 2021) and geochronological data discussed in the previous geological section provide evidence of rapid emplacement at shallow crustal levels (1-2 kb: Conte et al., 2017; Secchi et al., 2021) of a wide variety of compositionally different magma pulses: *(a)* mafic/granodiorite mingling relationships, the lack of contact metamorphic aureole and syn-magmatic deformation ; *(b)* granitic pulses that unconformably crosscut granodiorite flat intrusions with steep contacts; (*c*) undistinguishable ages, clustered at 286 Ma, based on several isotopic systematics on *stage 1* and *stage 2* units (Nicoletti et al., 1982; Di Vincenzo et al., 2005; Dack, 2009; Secchi et al., 2021); (*d*) occurrence of substantially coeval bimodal basaltic/rhyolitic dikes.

Stage 1 melt ascending is controlled by a dilatant roughly EW trending shear zone (the SSSZ) that acted as a feeder for magmas and records mingling relationships between granodiorites and gabbroic magmas. Indeed, the dilatant style of the SSSZ channelized the migration of large volumes of mantle-derived magmas up to upper crustal levels. Moreover, a close field association with peraluminous granites is observed (i.e., Monte Maria Unit; Fig. 2). Conversely, a succession of

independent granitic magma pulses that share a common F-rich ferroan character marks the *stage 2* (Fig. 5d). In this stage, mantle-derived magmas are only represented by few mafic dike swarms, representing a late generation of olivine-plagioclase phyric basalts with tholeiitic affinity (Ronca et al., 1999; Conte et al., 2017).

Petrogenetic constraints for Sàrrabus magmatism

Several lines of evidence support for the Sàrrabus pluton an early involvement of mantle-derived magmas and a progressive more relevant production of crustal-derived magmas. Overall, each rock-types shows distinctive petrographic and chemical characters which suggest independent evolution paths.

Petrographic data allow to constrain the evolution of different magma pulses to upper crustal levels. Evidence in favor of a general low-pressure evolution for mafic magmas hosted in Cala Regina Group (<5 kbar) is the early appearance of orthopyroxene followed by calcic plagioclase and clinopyroxene; in addition, olivine shows peritectic relationships with orthopyroxene (Conte et al., 2018a). The increase of water content in melts, testified by amphibole + dark mica segregation, characterizes the quartz gabbroic varieties; moreover, amphibole (Fe-hornblende) and dark mica of similar composition become the only mafic minerals within the assemblage of granodiorites.

Generation of different granitic magmas is constrained by the occurrence of garnet, muscovite and rare cordierite in Monte Maria Unit peraluminous rocks and, conversely, by the early appearance of hastingsite in metaluminous granites (Monte Sette Fratelli Unit). An upper limit of 5 kb for magma evolution (e.g., Green, 1977; Dahlquist et al., 2007 and references therein) is further confirmed for Monte Maria granite by homogeneous garnet compositions (spessartine contents > 10%), coexisting with cordierite.

Isotopic data constrain a general model for Sàrrabus magmatism. Sr–Nd systematics well document the contrasting behavior between two different groups of crustal-derived (peraluminous and metaluminous/subaluminous) granitic magmas and a small homogenous granodiorite field unrelated to the higher variation of the trend displayed by gabbroic magmas (Fig. 8). In addition, further evidence in favor of an independent origin between the mafic and granodioritic suites forming the Cala Regina Group is provided by serial affinity (Fig. 5*c*) and REE normalized patterns (Fig. 6*a*). In detail, the gabbroic rocks are generally LREE-enriched with respect to granodiorites; conversely, cumulitic varieties suggest that the segregation process for gabbroic parent melts produced a decrease in the LREE content. Granodiorites are more fractionated in LREE with respect to gabbroic rocks, but also show a more pronounced negative Eu anomaly, thus indicating that plagioclase fractionation in granodiorites has differently affected the REE compositions. The dual signature of gabbroic rocks pointing to none, or small segregation of plagioclase indicates

different *P-T* conditions for the parental melts during fractionation, thus suggesting a vertically zoned magmatic reservoir.

In a general extensional setting, the ascent of gabbroic magmas at middle/upper crustal levels may provide the necessary heat input to cause dehydration melting of biotite and muscovite in metasedimentary rocks and promotes the generation of peraluminous granitic melts belonging to the *stage 1*. In this scheme, evidence in favour of a source located in the middle crust is the general low-pressure (<5 kbar) evolution indicated for gabbroic magmas by textural relationships. In addition, generally flat REE patterns lead to exclude a garnet-bearing source.

As expected by geological relationships and petrographic characters, mafic and felsic dike swarms overlap the trends observed for rocks belonging to *stage 1* and *stage 2*, respectively.

A genetic model involving contamination and crystal/liquid fractionation process has been already proposed to explain the magmatic evolution observed for gabbroic magmas of Scala Carbonara body (SC in Fig. 2) contaminated by granodioritic magma (Poli and Tommasini, 1999). The different behavior of gabbroic and granodioritic magmas point to different compositions and evolutions of the parent melts. Overall, an enriched mantle source is inferred from Ta/Yb–Th/Yb plot for gabbroic magmas and for selected mafic dikes from Sàrrabus pluton, in agreement with data reported by Gaggero et al. (2007) for lamprophyric dikes from northern Sardinia (Supplementary Material Figure 5). In addition, mafic rocks of the Sàrrabus pluton shows several degrees of crustal assimilation as revealed by Rb, Ba, Th and U concentrations which are relatively high and negative εNd also in cumulate gabbroic rocks (Fig. 7). This implies consequences with regard to isotope ratios: Nd model ages for these rocks are actually meaningless, being calculated on mixed isotopic composition derived by several sources. Moreover, different isotopic trends displayed by gabbroic rocks and granodiorites suggest that the mantle-derived melts interacted with different crustal components and could be re-equilibrated at different crustal levels.

According to Conte et al. (2017), metaluminous to sub-aluminous granitic magmas require processes of partial melting involving lower crustal level of mostly intermediate/mafic composition, as confirmed by whole-rock initial Pb isotopic compositions of metaluminous to subaluminous granites (i. e., San Priamo and Monte Sette Fratelli units which plot in the lower crust field in the $^{206}Pb/^{204}Pb$–$^{208}Pb/^{204}Pb$ plot in Conte et al., 2017).

Evaluating the involvement of crustal materials

An essential assumption of our models of magma genesis and the relation to Nd isotopes is the involvement of pre-existing continental crustal material (with low εNd and relatively high Nd concentration) and/or contribution from sub-continental lithospheric mantle (SCLM) (with high εNd and moderate Nd concentration) in the generation of mafic and granitic magmas. The

$^{147}Sm/^{144}Nd$ ratio in a reservoir is expressed as the enrichment factor relative to CHUR as $f_{Sm/Nd} = (^{147}Sm/^{144}Nd_{sample})/(^{147}Sm/^{144}Nd_{CHUR}) - 1$ after De Paolo and Wasserburg (1976). According to De Paolo et al. (1992) the fractional isotopic shift from mantle (MC) to crustal (CC) εNd values can be described by the Neodymium Crustal Index (NCI): NCI = [εNd(rock) – εNd(MC)]/[εNd(CC) – εNd(MC)]. NCI thus describes the fraction of crustal Nd in a rock. NCI is 0 when the rock has no crustal Nd (the εNd value is equal to the mantle MC source value) and 1 when all Nd in a rock has a crustal origin (the εNd value is equal to the crustal CC value). Surveying local data, we have considered MC = +8 and CC = –15 for NCI calculation, representing MC – an average composition of the YMP mafic rocks from Sardinia (Gaggero et al., 2007), and CC – composition of the most crustal metasedimentary schist from the Sardinia basement (Di Vincenzo et al., 1996). Nd isotopic compositions of mafic/felsic rocks from Sàrrabus pluton and available data from entire Sardinia range from near model mantle values to near model crustal values (Fig. 9a). Moreover, collected data show slightly negative correlation in the $f_{Sm/Nd}$ vs. NCI plot, and partial coincidence of mafic rocks with granitic rocks. The abnormally high NCI = 0.62–0.75 for the mafic rocks was likely caused by fluid-metasomatism of pre-existing SCLM or related to contamination with (amphibolitic) lower crust. This enrichment is obvious from $f_{Sm/Nd}$ vs. $\varepsilon Nd_{(286)}$ plot (Shirey and Hanson, 1986; Fig. 9b) where both mafic and felsic rocks from Sàrrabus pluton lie in the quadrant characterized by crustal enrichment (i. e. negative $f_{Sm/Nd}$ and $\varepsilon Nd_{(i)}$ values; Fig. 9b).

Such mafic/felsic intrusions, that have initial Nd isotope ratios below to the chondritic value (εNd < 0), indicate possible SCLM sources that are chemically enriched/metasomatized, and thus different from the MORB or volcanic-arc basalt sources. Although the Sr–Nd isotopic characteristics of particularly mafic components are quite atypical, nevertheless it is possible to model the mixing between the mafic component (sample SSP6b from a mafic dike) and the crustal ones (sample SSP59, from peraluminous granite: Fig. 10). Obviously, from the presented model, the crustal source is dominant (80–85%) in the genesis of granodioritic magmas, as also supported by negative εHf(t) values, while the concomitant mafic components with unusually high negative $\varepsilon Nd_{(286)}$ over –4 (Fig.s 8 and 10) show considerable crustal enrichment or fluid-metasomatism.

This large involvement of crustal materials is coherent with negative εHf values of granodiorites zircons and the large compositional gap emerging from Sr–Nd systematics for Corsica and northern Sardinia granitoids with respect to Sàrrabus pluton (Fig. 8), that was inherited from deep sources of granite magmas and related to the thermal structure of different lithospheric fragments assembled during the Variscan collision in the Sardinia-Corsica massif. The more radiogenic signature and the value of $\delta^{18}O_{SMOW} = +8.4$ ‰ (Brotzu et al., 1981) observed for mafic suites and associated

granodiorites from Sàrrabus pluton does not conflict with an earlier contamination stage and different residence times at lower crustal levels with respect to the northern Sardinia/Corsica suites.

Mantle-crust interactions and nature of involved crustal materials

When considering the genesis and emplacement of Sàrrabus magmas, which belong to a reworked crust of the northern Gondwana margin thinned during the collapse and exhumation of the Variscan chain (Casini and Oggiano, 2008; Rossi et al., 2015), a complex petrological model can be depicted. Schematically, in a commonly accepted regime of lithospheric mantle delamination (Edel et al., 2014; Rossi et al., 2015), extensional shear zones, as the SSSZ, favoured the repeated ascents of mantle-derived magmas which experienced crystal/liquid fractionation (Poli and Tommasini, 1999; Conte et al., 2018; Franciosi et al., 2019) and likely served as a heat source for melting of metasedimentary crustal levels, producing peraluminous granite magmas in *stage 1*.

Tommasini et al. (1995) pointed out that the main geochemical characters of the Sardinian high-K and I-type calcalkaline granitoids suggest a dominant derivation from partial melting of metaigneous and igneous-derived materials belonging to a volcanic arc linked to an Ordovician subduction. Remarkably, this group of granites and rhyolitic dikes overlaps the field of felsic granulites belonging to the Central Spanish Variscan System (Villaseca et al., 1998); an overlap with lower crustal sources was also inferred by Pb isotopic data obtained for SPU leucogranites. According to Conte et al. (2017), granitic rocks like MSFU, which plot in the III quadrant of $^{87}Sr/^{86}Sr_t$ vs. $\varepsilon Nd_{(t)}$ diagram, have isotopic values which are rather uncommon at the scale of entire European Variscides.

Accordingly, the two-stage T_{DM} crustal residence ages calculated for Sàrrabus granites overlap those calculated for Cambro-Ordovician orthogneisses from northern Sardinia and central Iberia (Di Vincenzo and Ghezzo, 1996, Villaseca et al., 1998). On the other hand, the geochemical/metallogenic and lead isotopic signatures of the F-rich, ferroan granites indicates the derivation from meta-igneous sources in the lower crust (Conte et al., 2017). This provenience from a deep source for the metaluminous/subaluminous products of the Sàrrabus pluton *stage 2* may also assume the significance of a possible derivation from an inferred and more ancient (Proterozoic) volcanic arc, rooted in a crystalline basement under the cover of Paleozoic nappes.

Conclusions

The Sàrrabus pluton documents a sequence of magmatic events which record a repeated bimodal character in which different mantle-derived and crustal-related magmas, whose ascent was controlled by dilatant extensional faults, are recognized. Several lines of evidence suggest a

complex frame of mafic magmas promoting partial melting of continental crust, as well as continuous mafic/felsic magma interactions decreasing in time at different crustal levels. In the general late orogenic context of the frontal zone of the Variscan wedge, it is possible to hypothesize different scenarios capable of explaining thermal anomalies and magma production. Radiogenic heating of previous thickened crust and shear heating are mechanisms that can account for the heat supply consistent with generation of large volume of crustal melts. LID delamination is a further mechanism that from syn- to post- collisional settings can transfer large amount of heat from the mantle into the crust of evolving orogenic belts. Delamination models may be applied to the Variscan granitic provinces even in absence or scarcity of mantle magmas. Indeed, mixing processes, assimilation and mingled zones are clues for mantle contributes to the building of the Variscan batholiths, including the Corsica-Sardinia Batholith. The Sarrabus pluton intruded at 286 Ma in a slightly thickened frontal portion of the orogenic wedge, where low levels of radiogenic heating are expected and syn-intrusive shear heating is not documented. Therefore, these two heat sources can hardly account for the melting of the crust in this part of the Variscan chain. Conversely, the progressive migration of delamination away from the suture zone located in Northern Sardinia, down to Central-Southern Sardinia and Sàrrabus, could have heated the crust up to temperatures close to 1000 °C, which might lead to crustal melting at different crustal levels. A further hypothesis may consider the high heat flux produced by a possible lithosphere necking triggered by pre-existing weak zones in the mantle, determining astenospheric uplift to the crust base; the far field stress able to initiate necking in an already stiffed Variscan crust could be envisaged in the plate reorganization led to the Pangaea.

Whatever was the actual large-scale heating mechanism, stretching conditions of Sàrrabus crust favored the partial melting of different crustal levels by a heat input from mantle-derived gabbroic magmas. In this context a regime of decreasing temperature of the crust may account for the marked bimodality of diking activity, which inhibits the production of voluminous granodioritic magmas by mixing processes.

The following are the supplementary data related to this article.

Supplementary Material Table 1 -Selected chemical analyses for intrusives and mafic dikes from Sàrrabus pluton. Major (wt.%), trace elements (ppm) contents and petrochemical parameters
Supplementary Material Table 2 -Major (wt.%) and trace elements (ppm) contents for intrusives from Sàrrabus pluton
Supplementary Material Table 3 - Rb-Sr and Sm-Nd isotopic data for selected whole rock samples of early Permian intrusives and mafic dikes from Sàrrabus pluton (SE Sardinia. Italy)
Supplementary Material Table 4 -Lu-Hf isotopic data for selected zircons published by Secchi et al. (2021)
Supplementary Material Table 5 -Major (wt.%), trace elements (ppm) average contents for intrusives from Sàrrabus pluton[a]
Supplementary Figure 1
Supplementary Figure 2
Supplementary Figure 3
Supplementary Figure 4
Supplementary Figure 5

Acknowledgements

This work was supported by Fondo di Ateneo per la Ricerca -FAR2019- (Università di Sassari. Sassari, Italy), RAS L.R. 7/2007 research program 'Il blocco Sardo-Corso: area chiave per la ricostruzione della geodinamica Varisica' CUP J81G17000110002 and by RAS/FdS research program "Sustainable land management: the tools of geology for the environment" - CUP F75F21001270007). Special thanks to FO.RE.S.T.A.S. for the access to the natural reserve of Monte Sette Fratelli, to Mattia Alessio Meloni for some outcrop pictures and to Daniele De Lisa for part of the graphic work.

Declaration of interests

The authors declare that they have no known competing financial interests or personal relationships that could have appeared to influence the work reported in this paper.

The authors declare the following financial interests/personal relationships which may be considered as potential competing interests

REFERENCES

1. Avanzinelli, R., Boari, E., Conticelli, S., Francalanci, L., Guarnieri, L., Perini, G., Petrone, M.C., Tommasini, S., Ulivi, M. (2005). High precision Sr, Nd and Pb isotopic analyses using the new generation Thermal Ionisation Mass Spectometer ThermoFinnigan Triton-Ti®. Periodico di Mineralogia, 74(3), 147-166.
2. Barbey, P., Gasquet, D., Pin, C., Bourgeix, A. L. (2008). Igneous banding, schlieren and mafic enclaves in calcalkaline granites: The Beddduso pluton (Sardinia). Lithos, 104, 147-163.
3. Baxter, S., Feely, M. (2002). Magma mixing and mingling textures in granitoids: Examples from the Galway Granite, Connemara, Ireland. Mineralogy and petrology, 76, 63-74. DOI:10.1007/s007100200032.
4. Bosi, F., Naitza, S., Secchi, F., Conte, A. M., Cuccuru, S., Andreozzi, G. B., Skogby, H., Hålenius, U. (2019). Petrogenetic controls on the origin of tourmalinite veins from Mandrolisai igneous massif (central Sardinia, Italy): Insights from tourmaline crystal chemistry. Lithos. 342–343, 333–344.
5. Brotzu, P., Ferrini, V., Masi, U. (1983). Stable isotope geochemistry of Hercynian granitoid rocks from the Sarrabus massif (southeastern Sardinia, Italy). Chemical Geology, 41, 77–90.
6. Brotzu, P., Callegari, E., Secchi, F. (1993). The search for the parental magma of the high-K calcalkaline igneous rocks series in the southernmost Sardinia batholith. Periodico di Mineralogia, 63, 253-280.
7. Carmignani, L., Carosi, R., Di Pisa, A., Gattiglio, M., Musumeci, G., Oggiano, G., Pertusati, P. C. (1994). The Hercynian chain in Sardinia (Italy). Geodinamica Acta, 7, 31-47. doi.org/10.1080/09853111.1994.11105257.
8. Casini, L., Funedda, A. (2014) – Potential of pressure solution for strain localization in the Baccu Locci Shear Zone (Sardinia, Italy). Journal of Structural Geology, 66, 188-204. doi: 10.1016/j.jsg.2014.05.016
9. Casini, L., Oggiano, G. (2008). Late orogenic collapse and thermal doming in the northern Gondwana margin incorporated in the Variscan Chain: a case study from the Ozieri Metamorphic Complex, northern Sardinia, Italy. Gondwana Research, 13, 396-406.
10. Casini, L., Cuccuru, S., Maino, M., Oggiano, G., Tiepolo, M. (2012). Emplacement of the Arzachena pluton (Corsica-Sardinia batholith) and the geodynamics of the incoming Pangea. Tectonophysics, 544–545, 31–49. doi.org/10.1016/j.tecto.2012.03.028.
11. Casini, L., Cuccuru, S., Maino, M., Oggiano, G., Puccini, A., Rossi, P. (2015a). Structural map of Variscan northern Sardinia (Italy). Journal of Maps, 11(1), 75-84. doi: 10.1080/17445647.2014.936914.

12. Casini, L., Cuccuru, S., Puccini, A., Oggiano, G., Rossi, Ph. (2015b). Evolution of the Corsica–Sardinia batholith and late-orogenic shearing of the Variscides. Tectonophysics, 646, 65–78. doi.org/10.1016/j.tecto.2015.01.017.
13. Clemens, J. D., Wall, J. V. (1981). Origin and crystallization of some peraluminous (S-type) granitic magmas. Canadian Mineralogist, 19, 111–131.
14. Cocherie, A., Rossi, Ph., Fouillac, A.M., Vidal, Ph. (1994). Crust and mantle contributions to granite genesis -an example from the Variscan batholith of Corsica, France, studied by trace element and Nd-Sr-O-isotope systematics. Chemical Geology, 115, 173–211. doi.org/10.1016/0009-2541(94)90186-4.
15. Cocherie, A., Rossi, P., Fanning, C. M., Guerrot, C. (2005). Comparative use of TIMS and SHRIMP for U–Pb zircon dating of A-type granites and mafic tholeiitic layered complexes and dykes from the Corsican Batholith (France). Lithos, 82, 185-219. doi: 10.1016/j.lithos.2004.12.016.
16. Conte, A. M., Cuccuru, S., D'Antonio, M., Naitza, S., Oggiano, G., Secchi, F., Casini., L., Cifelli, F. (2017). The post-collisional late Variscan ferroan granites of southern Sardinia (Italy): Inferences for inhomogeneity of lower crust. Lithos, 294–295, 263–282. doi.org/10.1016/j.lithos.2017.09.028.
17. Conte, A. M., Naitza, S., Oggiano, G., Secchi, F., Cuccuru, S., Casini, L., Puccini, A. (2018a). Architecture, emplacement mode of late-Variscan plutons and their relationships with post-collisional phases: examples from Sarrabus igneous massif (SE Sardinia, Italy). Abstract book Congresso congiunto SIMP-SGI, Catania, 12-14 settembre 2018. doi.org/10.3301/ABSGI/2018.02.
18. Conte, A. M., Cuccuru, S., D'Antonio, M., Naitza, S., Oggiano, G., Secchi, F. (2018b). Long-lasting mantle-derived activity and evolution in the late-Variscan Sarrabus igneous complex (SE Sardinia, Italy). Abstract book Congresso congiunto SIMP-SGI, Catania, 12-14 settembre 2018. doi.org/10.3301/ABSGI/2018.02.
19. Cortesogno, L., Cassinis, G., Dallagiovanna, G., Gaggero, L., Oggiano, G., Ronchi, a., Seno, S., Vsnossi, M. (1998). The Variscan post-collisional volcanism in Late Carboniferous–Permian sequences of Ligurian Alps, Southern Alps and Sardinia (Italy): a synthesis. Lithos, 45, 305-328. https://doi.org/10.1016/S0024-4937(98)00037-1.
20. Cruciani, G., Franceschelli, M., Groppo C., Oggiano, G., Spano, M. E. (2015)- Re-equilibration history and P–T path of eclogites from Variscan Sardinia, Italy: a case study from the medium-grade metamorphic complex. International Journal of Earth Sciences, 104, 797–814.
21. Cuccuru, S., Naitza, S., Secchi, F., Puccini, A., Casini, L., Pavanetto, P., Linnemann, U., Hofmann M., Oggiano, G. (2016). Structural and metallogenic map of late Variscan Arbus igneous complex (SW Sardinia, Italy). Journal of Maps, 12, 860–865.
22. Dack, A.V. (2009). Internal Structure and Geochronology of the Gerrei Unit in the Flumendosa Area, Variscan External Nappe Zone, Sardinia, Italy. M. A. Thesis., Boise State University. Idaho, USA.
23. Dahlquist, J.A., Galindo, C., Pankhurst, R.J., Rapela, C.W., Alasino, P.H., Saavedra, J., Fanning, C.M. (2007). Magmatic evolution of the Peñón Rosado granite: Petrogenesis of garnet-bearing granitoids. Lithos, 95, 177-207.
24. D'Angelo, R. (1998). Rilevamento e caratterizzazione petrografica delle masse basiche del settore Geremèas-Monte Turnu (Sàrrabus, Sardegna sud-orientale). M.Sc. Thesis. Università degli Studi di Cagliari. 1-127.
25. DePaolo, D. J., Wasserburg, G. J. (1976). Nd isotopic variations and petrogenetic models. Geophysical Research Letters, 3, 249–252. https://doi.org/10.1029/GL003i005p00249.
26. DePaolo, D. J., Perry, F. V., Baldridge, W. S. (1992). Crustal versus mantle sources of granitic magmas: a two-parameter model based on Nd isotopic studies. Transactions of the Royal Society of Edinburgh: Earth Sciences, 83, 439–446.
27. Dini, A., Di Vincenzo, G., Ruggieri, G., Rayner, J., Lattanzi, P. (2005). Monte Ollasteddu, a new gold discovery in the Variscan basement of Sardinia (Italy): first isotopic (40Ar−39Ar, Pb) and fluid inclusion data. Mineralium Deposita, 40, 337–346.
28. Di Vincenzo, G., Andriessen, P. A., Ghezzo, C. (1996). Evidence of Two Different Components in a Hercynian Peraluminous cordierite bearing granite: the San Basilio Intrusion (Central Sardinia, Italy). Journal of Petrology, 37, 1175-1206. doi.org/10.1093/petrology/37.5.1175.
29. Downes, H. and Leyreloup, A. F. (1986). Granulitic xenoliths from the French Massif Central: petrology, Sr and Nd isotope systematic and model ages estimates. Geological Society London Special Publications, 24, 319–330.

30. Downes, H., Shaw, A., Williamson, B.J., Thirlwall, M. F. (1997). Sr, Nd and Pb isotopic evidence for the lower crustal origin of Hercynian granodiorites and monzogranites, Massif Central, France. Chemical Geology, 136, 99–122.
31. Edel, J. B., Casini, L., Oggiano, G., Rossi, P., Schulmann, K. (2014). Early Permian 90° clockwise rotation of the Maures–Esterel–Corsica–Sardinia block confirmed by new palaeomagnetic data and followed by a Triassic 60° clockwise rotation. Geological Society London Special Publications, 405, 333–361. doi: 10.1144/SP405.10.
32. Edel, J. B., Schulmann, K., Lexa, O., Diraison, M., Géraud, Y. (2015). Permian clockwise rotations of the Ebro and Corso-Sardinian blocks during Iberian–Armorican oroclinal bending: Preliminary paleomagnetic data from the Catalan Coastal Range (NE Spain). Tectonophysics, 657, 172-186.
33. Ferré, E. C. and Leake, B. E. (2001). Geodynamic significance of early orogenic high-K crustal and mantle melts: example of the Corsica Batholith. Lithos, 59(1-2), 47-67. doi: 10.1016/s0024-4937(01)00060-3.
34. Franciosi, L., D'Antonio, M., Fedele, L., Guarino, V., Tassinari, C. C. G., de Gennaro, R., Cucciniello, C. (2019). Petrogenesis of the Solanas gabbro-granodiorite intrusion, Sàrrabus (southeastern Sardinia, Italy): implications for Late Variscan magmatism. International Journal of Earth Sciences, 108, 989-1012. DOI: 10.1007/s00531-019-01689-6
35. Franzini, M., Leoni, L., Saitta, M. A. (1972). A simple method to evaluate the matrix effects in X-ray fluorescence analysis. X-Ray Spectrometry, 1 (4), 151–154.
36. Frost, B. R., Barnes, C. G., Collins,W. J., Arculus, R. J., Ellis, D. J., Frost, C. D. (2001). A geochemical classification for granitic rocks. Journal of Petrology, 42, 2033–2048.
37. Funedda, A., Naitza, S., Buttau, C., Cocco, F., Dini, A. (2018). Structural controls of ore mineralization in a polydeformed basement: field examples from the Variscan Baccu Locci shear zone (SE Sardinia, Italy). Minerals, 8(10), 456. https://doi.org/10.3390/min8100456
38. Gaggero, L., Oggiano, G., Buzzi, L., Slejko, F., Cortesogno, F. (2007). Post-Variscan mafic dikes from the late orogenic collapse to the Tethyan rift: evidence from Sardinia. Ofioliti, 32, 15–37.
39. Gaggero, L., Oggiano, G., Funedda, A., Buzzi, L. (2012). Rifting and arc-related early Paleozoic volcanism along the north Gondwana margin: geochemical and geological evidence from Sardinia (Italy) The Journal of Geology, 120, 273-292. https://doi.org/10.1086/664776
40. Gaggero, L., Gretter, N., Langone, A., Ronchi, A. (2017). U–Pb geochronology and geochemistry of late Palaeozoic volcanism in Sardinia (southern Variscides). Geoscience Frontiers, 8, 1263-1284. https://doi.org/10.1016/j.gsf.2016.10.005.
41. Giovanardi, T. and Lugli, F. (2017). The Hf-INATOR: A free data reduction spreadsheet for Lu/Hf isotope analysis. Earth Science Information, 10, 517–523.
42. Giovanardi, T.; Mazzucchelli, M.; Lugli, F.; Girardi, V.A.; Correia, C.; Tassinari, C.C.; Cipriani, A. (2018) Isotopic constraints of contamination processes in the Tonian Goiás Stratiform Complex. Lithos, 310, 136–152.
43. Green, T.H. (1977). Garnet in silicic liquids and its possible use as a P-T indicator. Contributions to Mineralogy and Petrology, 65, 59-67.
44. Hart, S.R., Blusztajn, J., Dick, H.J.B., Meyer, P.S., Muehlenbachs, K. (1999). The fingerprint of seawater circulation in a 500-meter section of ocean crust gabbros. Geochimica et Cosmochimica Acta, 63, 4059–4080.
45. Hodkinson, D., Krogstadt, E. J., Brown, M. (1995). Geochemical constraints on magma sources of Mesozoic continental arc plutonic complexes, Andean plate boundary zone, North Chile. In The origin of granites and related rocks. Third Hutton. Symposium, College Park, M. D,66-67.
46. Janoušek, V., Rogers, G., Bowes, D.R. (1995). Sr-Nd isotopic constraints on the petrogenesis of the Central Bohemian Pluton, Czech Republic. Geologische Rundschau, 84, 520–534.
47. Janoušek, V., Moyen, J. F., Martin, H., Erban, V., & Farrow, C. (2016). Geochemical modelling of igneous processes: principles and recipes in R language. Bringing the Power of R to a Geochemical Community. Springer-Verlag, Berlin, Heidelberg. ISBN 978-3-662-46792-3.
48. Kröner, A. Willner, P. (1998). Time of formation and peak of Variscan HP-HT metamorphism of quartz-feldspar rocks in the central Erzgebirge, Saxony, Germany. Contributions to Mineralogy and Petrology, 132, 1–20.
49. Lu, S., Zhu, X., Li, X. (2019). Geochronology and geochemistry of the five magmatic rocks in the Ningzhen region, China. Acta Geochimica, 38(02), 241-261. https://doi.org/10.1007/s11631-019-00316-2.

50. Ludwig, K. R. (2012). Isoplot 3.75. A geochronological toolkit for Microsoft Excel. Berkeley Geochronology Center. Special publication, 5.
51. Matte, P. (2001). The Variscan collage and orogeny (480-290 Ma) and the tectonic definition of the Armorica microplate. Terra Nova, 13, 122-128.
52. McDonough, W. F., Sun, S.S. (1995). The composition of the Earth. Chemical Geology, 120, 223–253.
53. Meloni, M. A., Oggiano, G., Funedda, A., Pistis, M., Linnemann, U. (2017). Tectonics, ore bodies, and gamma-ray logging of the Variscan basement, southern Gennargentu massif (Central Sardinia, Italy). Journal of maps, 13, 196–206.
54. Miller, C. F. (1985). Are strongly peraluminous magmas derived from pelitic sedimentary sources? Journal of Geology, 93, 673–689.
55. Musumeci, G., Spano, M. E., Cherchi, G. P., Franceschelli, M., Pertusati, P. C., Cruciani, G. (2014). Geological Map of the Monte Grighini Variscan Complex (Sardinia, Italy). Journal of Maps, 287-298 https://doi.org/10.1080/17445647.2014.924441.
56. Naitza, S., Conte, A.M., Cuccuru, S., Oggiano, G., Secchi, F., Tecce, F. (2017). A Late Variscan tin province associated to the ilmenite-series granites of the Sardinian Batholith (Italy): the Sn and Mo mineralisation around the Monte Linas ferroan granite. Ore Geology Reviews, 80, 1259–1278.
57. Nicoletti, M., Ardanese L. R., Colasanti, S. (1982). La granodiorite di Capo Carbonara (Sardegna-Italia). Età K-Ar di fasi minerali in paragenesi. Rendiconti Società Italiana di Mineralogia e Petrologia, 38(2), 765-769.
58. Oggiano, G., Gaggero, L., Funedda, A., Buzzi, L., Tiepolo, M. (2010). Multiple early Paleozoic volcanic events at the northern Gondwana margin: U–Pb age evidence from the Southern Variscan branch (Sardinia, Italy). Gondwana Research, 17, 44–58.
59. Paquette, J. L., Ménot, R.-P., Pin, C., Orsini, J. B. (2003). Episodic and short-lived granitic pulses in a post-collisional setting: evidence from precise U–Pb zircon dating through a crustal cross-section in Corsica. Chemical Geology, 198 (1-2), 1-20. doi: 10.1016/s0009-2541(02)00401-1.
60. Pirinu, N. (1994). Le sieniti del Sàrrabus meridionale (Sardegna SE). Unpublished PhD thesis, University of Napoli. 1-81.
61. Poli, G., Ghezzo, C., Conticelli, S. (1989). Geochemistry of granitic rocks from the Hercynian Sardinia-Corsica batholith: Implication for magma genesis. Lithos, 23(4), 247-266. doi: 10.1016/0024-4937(89)90038-8.
62. Poli, G., Tommasini, S. (1999). Geochemical modelling of acid-basic magma interaction in the Sardinia-Corsica Batholith: the case study of Sàrrabus, southeastern Sardinia, Italy.Lithos 46, 553-571.
63. Puccini, A., Xhixha, G., Cuccuru, S.,1, Oggiano, G., Kaçeli Xhixha, M., Mantovani, F., Rossi Alvarez, C., Casini, L. (2013). Radiogenic heat potential of the Sardinian Variscan crust. Goldschmidt 2013 Conference Abstracts. 2002
64. Renna, M. R., Tribuzio, R., Tiepolo, M. (2006). Interaction between basic and acid magmas during the latest stages of the post-collisional Variscan evolution: clues from the gabbro–granite association of Ota (Corsica–Sardinia batholith). Lithos, 90, 92–110. doi:10.1016/j.lithos.2006.02.003.
65. Ronca, S., Del Moro, A., Traversa, G. (1999). Geochronology, Sr-Nd isotope geochemistry and petrology of Late Hercynian dike magmatism from Sarrabus (SE Sardinia). Periodico di Mineralogia, 68, 231–260.
66. Rossi, Ph., Cocherie, A. (1991). Genesis of a Variscan batholith: field, petrological and mineralogical evidence from the Corsica-Sardinia batholith. Tectonophysics, 195, 319–346.
67. Rossi, Ph., Oggiano, G., Cocherie, A. (2009). A restored section of the "southern Variscan realm" across the Corsica–Sardinia microcontinent. Comptes Rendus Geoscience 341, 224–238.
68. Rossi, Ph., Cocherie, A., Fanning, C. M. (2015). Evidence in Variscan Corsica of a brief and voluminous Late Carboniferous to Early Permian volcanic-plutonic event contemporaneous with a high-temperature/low-pressure metamorphic peak in the lower crust. Bulletin de la Société Géologique de France, 186, 171–192. doi.org/10.2113/gssgfbull.186.2-3.171.
69. Secchi, F., Brotzu, P., Callegari, E. (1991). The Arburèse igneous complex (SW Sardinia, Italy) –an example of dominant igneous fractionation leading to peraluminous cordierite-bearing leucogranites as residual melts. In: A. Peccerillo (Ed.), Geochemistry of granitoid Rocks. Chemical Geology, 92, 213–249.

70. Secchi, F., Naitza, S., Oggiano, G., Cuccuru, S., Puccini, A., Conte, A. M., Giovanardi, T., Mazzucchelli, M., 2021. Geology of late-Variscan Sàrrabus pluton (south-eastern Sardinia, Italy). Journal of maps. 17, https://doi.org/10.1080/17445647.2021.1982032.
71. Shirey, S. B., Hanson, G. N. (1986). Mantle heterogeneity and crustal recycling in Archean granite-greenstone belts: evidence from Nd isotopes and trace elements in the Rainy Lake area, Superior Province, Ontario, Canada. Geochimica et Cosmochimica Acta, 50, 2631–2651. https://doi.org/10.1016/0016-7037(86)90215-2
72. Stampfli, G. M., von Raumer, J., Borel, G. (2002). The paleozoic evolution of pre-Variscan terranes: From Gondwana to the Variscan collision. Geological Society of America, 364, 263–280.
73. Stormer, J. C., Nicholls, J., 1978. XLFRAC: a program for the interactive testing of magmatic differentiation models. Computers and Geosciences 4, 143–159.
74. Thirwall, M. F. (1991). Long-term reproducibility of multicollector Sr and Nd isotope ratio analysis1. Chemical Geology, 94, 85-104. https://doi.org/10.1016/S0009-2541(10)80021-X
75. Tommasini, S., Poli, G. (1992). Petrology of the late-Carboniferous Punta Falcone gabbroic complex, northern Sardinia, Italy. Contribution to Mineralogy and Petrology, 110, 16–32.
76. Tommasini, S., Poli, G., Halliday, A. N. (1995). The role of sediment subduction and crustal growth in Hercynian plutonism: isotopic and trace element evidence from the Sardinia–Corsica Batholith. J. Petrol. 36, 1305–1332.
77. Villaseca, C., Barbero, L., Rogers, G. (1998). Crustal origin of Hercynian peraluminous granitic batholiths of Central Spain: petrological, geochemical and isotopic (Sr, Nd) constraints. Lithos, 43, 55–79.
78. Villaseca, C., Pérez-Soba, C., Merino, E. M., Orejana, D., López-García, J. A., Billstrom, K. (2008) Contrasted crustal sources for peraluminous granites of the segmented Montes de Toledo Batholith (Iberian Variscan Belt). Journal of Geosciences, 53, 263–280. DOI: http://dx.doi.org/10.3190/jgeosci.035
79. Woodhead, J.D. and Hergt, J.M. (2005), A Preliminary Appraisal of Seven Natural Zircon Reference Materials for In Situ Hf Isotope Determination. Geostandards and Geoanalytical Research, 29: 183-195. https://doi.org/10.1111/j.1751-908X.2005.tb00891.x
80. Zorpi, M. J., Coulon, C., Orsini, J. B. (1991). Hybridization between felsic and mafic magmas in calcalkaline granitoids a case study in northern Sardinia, Italy. Chemical Geology, 92, 45-86.

Fig. 1: simplified geological map of Sardinia-Corsica batholith (after Casini et al., 2012). 1-4: metamorphic basement. (1) Pan-African schists. (2) Unmetamorphosed Foreland. (3) Low- to medium-grade metamorphic units (nappe zone). (4) High grade metamorphic complex. 5-6 Sardinia-Corsica batholith. (5) Syn-collisional Variscan magmatism (Mg-K rock-series). (6) Late-Variscan post-collisional magmatism. (7) Post-Variscan covers. Other symbols: main Variscan faults (8). From north to south, Arg, SM, Arz, Br, Gn, Gh, Arb and SV refer to localities cited in the text (Santa Maria Island, Arzachena, Barrabisa, Gennargentu, Grighini, Arburèse and San Vito, respectively).

Fig. 2: Geological sketch map of late-Variscan Sàrrabus pluton (SE Sardinia, Italy). (1) Undifferentiated epimetamorphic complex: metasandstones, metapelites and metalimestones (Cambrian-early Carboniferous). (2-8) Late-Variscan igneous units of Sàrrabus pluton: (2) Two-pyroxene biotite gabbro tonalites (Burcèi Unit). (3) biotite to biotite hornblende granodiorites (Cala Regina Group) with syn-plutonic stocks and dismembered dikes of two pyroxene-bearing hornblende gabbroic varieties (Solànas complex; SO). (4) Garnet-bearing two mica granites (Monte Maria Unit). (5) biotite monzogranites grading to leucogranites (Bruncu Nicola Bove Unit). (6) F-rich biotite leucogranite (San Priamo Unit). (7) F-rich hastingsite granite stocks (Monte Sette Fratelli Unit). (8) Mafic and acidic dike swarms. (9) Post-Mesozoic sedimentary and volcanic covers and recent continental and transitional sedimentary deposits. Other symbols (10-12). Late-Variscan southern Sàrrabus shear zone (SSSZ) (10). Main extensional faults, certain (11) and inferred/buried (12). CR, Ge, TF, So, SC, Vs, Ca, S.P., Bu, S.G. and M. SF refer to Cala Regina, Geremèas, Torre de su Fenugu, Solànas, Scala Carbonara, Villasimìus, Castiadas, San Priamo, Burcei, San Gregorio and Monte Sette Fratelli localities cited in the text, respectively.

Fig. 3: Field relationships of Sàrrabus igneous rocks. (a) Sub-horizontal magmatic foliation of hornblende granodiorites evidenced by dark and felsic enclaves (FE; Capo Carbonara). (b) strongly foliated quartz diorites with large mafic enclaves of quartz gabbroic composition (Porto Murròni); (c) densely interdigitation between gabbroic rocks and quartz diorites (western slope of Torre de su Fenùgu); (d) disrupted large syn-magmatic mafic dikes into granodiorite (western slope of Torre de su Fenùgu); (e) contact relationships between different dike generation: composite dikes predate metaluminous acidic dikes (Cala Regina); (f) fine-grained centimetric rounded dark enclaves in acidic dike (Porto Murròni).

Fig. 4: Petrographical characters of magmatic rocks from Sàrrabus igneous massif. (a) two pyroxene-bearing equigranular gabbroic rocks from inner part of Scala Carbonara body (crossed polars; Scala Carbonara, sample SSP16,); (b) panidiomorphic textures of quartz microgabbros (crossed polars; sample SSP17; Capo Carbonara); (c) cumulophyric texture of olivine-bearing dark layers from stratified septa (crossed polars; Cabu Oi, sample SSP29); (d) clinopyroxene/brown amphibole relationships in equigranular varieties of mafic dike (crossed polars; north of Olia Speciosa, sample ESP10); (e) local plagioclase enriched zones in hornblende quartz diorites (crossed polars; sample SSP8, Porto Murroni; (f) large patchy-zoned plagioclase lath on Cala Regina granodiorites (crossed polars; Monte Nai, sample ESP1), (g) interstitial white mica in San Priamo leucogranites of (plane polarized light; Monte Gruttas, sample SPP9); (h) Almandine garnet associated to pinitized cordierite in peraluminous granites of Monte Maria Unit (plane polarized light; Porto Carbonara, sample LPC).

Fig. 5: Discrimination diagrams for the igneous rocks from Sàrrabus pluton. (a) Boundaries according to Peccerillo and Taylor (1976); (b) discrimination diagram for basaltic rocks. HAB and HMB refer to high alumina and high Mg basalts respectively; boundaries according to Miyashiro (1974). (c) and (d) Frost's and Frost (2001) discrimination diagrams. C, CA, AC and A refer calcic, calc-alkalic, alkali-calcic and alkaline rock-series, respectively. Pale and smaller symbols refer to literature data. Literature after Poli and Tommasini (1999) and Franciosi et al. (2019) is reported for comparison. Fields refer to mafic and acidic dike swarms (data after Ronca et al., 1999).

Fig. 6: REE normalized patterns for Sàrrabus magmatism: (a) syn-plutonic gabbroic suite; solid, double and dashed lines refer to olivine-bearing cumulate, two pyroxene-bearing gabbros and hornblende Qz-gabbros, respectively. Light and pale blue fields refer to data for olivine-bearing cumulates and hornblende Qz-gabbros (Franciosi et al., 2019), respectively. (b) Granodiorite rock-association; solid, double and dashed lines refer to Qz-diorite, tonalitic granodiorite and foliated granodiorite, respectively. The solid field refers to data for granodiorites after Franciosi et al. (2019); (c) mafic dikes; solid field refers to data for basalts from Ronca et al. (1999); (d) granites and felsic dikes; solid, dashed and dotted lines refer to peraluminous granite, metaluminous dikes and peraluminous dike (data after Ronca et al., 1999), resepctively. Dark and pale yellow solid fields refer to San Priamo and Monte Sette Fratelli granites, respectively (data after Conte et al. (2017). Data are normalized to CI (Mc Donough and Sun, 1995). Labels in (c) as in Supplementary Material Table 1.

Fig. 7: Spider diagrams for syn-plutonic mafic (a) and granodiorite (b) rock-associations from Sàrrabus pluton normalized to primitive mantle (McDonough and Sun, 1995). Peraluminous granite is reported for comparison.

Fig. 8: $\varepsilon Nd_{(t)}$ vs. $^{87}Sr/^{86}Sr_{(t)}$ for late-Variscan rocks from Sàrrabus pluton (south-eastern Sardinia, Italy) calculated for an age of 286 Ma (see text). Red, orange, and blue colors refer to Corsica, Gallura (northern Sardinia) and Sàrrabus pluton, respectively. Circle refer to peraluminous garnet-bearing granite from Monte Maria Unit. Barred circles refer to metaluminous to sub-aluminous granites of San Priamo and Monte Sette Fratelli units (data after Conte et al., 2017). Dike trend

refers to mafic to intermediate dikes from Sàrrabus pluton (data after Ronca et al., 1999). Data for Corsica mafic suites after Cocherie et al. (1994); data for Gallura mafic suites after Tommasini et al., 1995 (Punta Falcone) and Casini (Bortigiadas and La Etica), still unpublished data; mafic (subalkaline and transitional) dikes after Gaggero et al., 2007). Dark blue arrow refers to gabbros to hornblende quartz micro gabbros evolutive line (with olivin-cumulites at left hand). Note the position of granodiorites outside of evolutive sequence and the intermediate position of tonalites for which a hybrid origin is required. Note also that less evolved granodiorites (i.e., Scala Carbonara and Capo Carbonara) show a more radiogenic character with respect of Solànas granodiorites (Porto Murroni).

Fig. 9: a) f(Sm/Nd) vs. NCI plot for the Sàrrabus pluton and other available Sardinia samples. fSm/Nd = ($^{147}Sm/^{144}Nd_{sample}$)/($^{147}Sm/^{144}Nd_{CHUR}$) – 1 (DePaolo and Wasserburg, 1976); NCI = [εNd(rock) – εNd(MC)] / [εNd(CC) – εNd(MC)] according DePaolo et al. (1992). Field refer to metasediments from central-eastern Sardinia (data after Di Vincenzo et al., 1996). b) f(Sm/Nd) vs. $\varepsilon Nd_{(286)}$ plot for the Sàrrabus pluton and other available Sardinia sample. DM, EM and CC are according to Hodkinson et al. (1995). Field refer to orthogneisses and migmatites from central-eastern Sardinia (data after Di Vincenzo et al., 1996). Other symbols as in Fig. 5.

Fig. 10: Mixing binary plot of $^{87}Sr/^{86}Sr_{(286)}$ vs. $\varepsilon Nd_{(286)}$ showing variability of rocks from Sàrrabus pluton. Symbols as in Fig. 5 and 10; numbers refer to SSP samples reported in Supplementary Material Table 3. Dashed lines refer to possible mixing hyperbolas obtained by reverse least-squares method (Janoušek et al., 2016) using SSP6b (mafic dike) and SSP59 (peraluminous granite) samples as mantle- and crustal-derived endmembers, respectively to model the observed granodiorite rock-association. Pale field refer to data for granodiorite rock-association after Poli and Tommasini (1999) and Franciosi et al. (2019).

Tab. 1 -*Summary of petrographic features for late-Variscan intrusives and dikes from Sàrrabus igneous massif (south-eastern Sardinia, Italy)*

	Rock-types	*Rock-textures*	*Fundamental phases*	*Accessory phases*	*Late-stage*
	Latest mafic dikes (tholeiitic basalts)	Porphyritic Sub ophitic	Ol + Pl → Cpx + Pl ± Hbl Pl + Cpx ± Ol + Qz	Ti-Mt + Ilm + Sulf + Ap	Tc + Cc
	Mafic dikes (basalts to andesites)	Porphyritic to hypidiomorphic	Pl + Hbl + Qz ± Bt ± Opx ± Cpx	Ti-Mt + Ilm + Sulf + Ap ± All	
	Felsic dikes	Microgranular to granophyric	Qz + Kfs + Pl + Bt	Zrn + Ap + All + Mnz + Ilm + Mt	Fl
Stage 2	*Leucogranites to monzogranites (BNB, SP and SF)*	*SF*:	Qz + Kfs + Pl + Hs + Ann	Aln + Mt + Zrn + Ap	Fl + Ann
		Hypidiomorphic *SP*:	Qz + Kfs + Pl + Bt	Aln + Mt + Zrn	Bt + Ms + Fe-Chl
		BNB:	Qz + Kfs + Pl + Bt	Ilm + Ap + Zir	
Stage 1	*Peraluminous felsic dikes*	Microgranular/porphyritic	Qz + Kfs + Pl + Bt ± Ms ± And	Ilm + Zrn + Ap ± Mnz	Tum

Peraluminous granite (MM)	Hypidiomorphic	Qz + Kfs + Pl + Bt + Gt + Ms ± Chrd	Ilm + Zrn + Ap ± Mnz	
Gabbroic rocks (CR)	Hypidiomorphic Panhydiomorphic/Hypidiomorphic Pecilophytic	Mg-Hbl + Pl + Bt + Qz ± Opx ± Cpx Pl + Mg-Hbl + Bt + Qz ± Kfs ± Opx Ol + Opx +Cpx + Pl + Qz	Tit + Mt+ Ap + Ilm Ilm+Tit+All+Zrn Mt + Ap	Actin+Cumm Cumm Actin+Prgs
Granodiorites (CR))	Hypidiomorphic	Pl + Kfs + Qz + Fe-Hbl + Bt	Ilm + Ap + Aln + Mon ±Tit	Turm
	Hypidiomorphic	Qz + Kfs + Pl + Bt ± Fe-Hbl	Ilm + Zrn + Ap	Turm
Gabbrotonalites (BU)	Hypidiomorphic Porphyritic	Pl + Qz + Kfs + Bt + Opx + Cpx Pl + Opx + Cpx + Hbl → Pl + Bt + Kfs + Qz	Ilm + Ap + Zrn + Sulf	Actin+Cumm

CR, BU, MM, BNB, SP and SF refer to, Cala Regina Group and Burcèi, Monte Maria, Bruncu Nicola Bove, San Priamo and Monte Sette Fratelli rock-units reported in Fig. 2. Abbreviations list for mineral phases: Pl = plagioclase; Qz = quartz; Kfs = K-feldspar; Bt = biotite; Hbl = hornblende; Opx = orthopyroxene; Cpx = clinopyroxene; Hs = hastingsite; Gt = garnet; Ms = white mica; And = andalusite; Chrd = cordierite; Ol = olivine; Ilm = ilmenite; Ap = apatite; Mon = monazite; Aln = allanite; Zrn = zircon; Sulph = sulphides; Mt = magnetite; Alb = albite: Fl = fluorite; Ann = annite; Actin = actinolite; Cumm = cummingtonite; Prgs = pargasite; Fe-Chl = Fe-chlorite; Tc = talc. Talc observed in mafic dikes formed at the expense of olivine phenocrysts. Ortho- and clinopyroxene observed in Burcèi gabbrotonalites and gabbroic rocks belonging to Stage 1 show commonly a hypersthene and augitic composition, respectively; they are often replaced by actinolite and cummingtonite.

Highlights

- The Sàrrabus pluton is formed by multiple short-lived intrusions at ca. 286 Ma;
- Pluton growth started with an early stage of broadly granodioritic composition;
- Large intrusions of metaluminous to subaluminous granites follow the granodiorites;
- During the pluton growth, a progressive increase in crustal magmas generation occurred;
- Last magmatics are subalkaline mafic/felsic dikes with major intrusions signature;

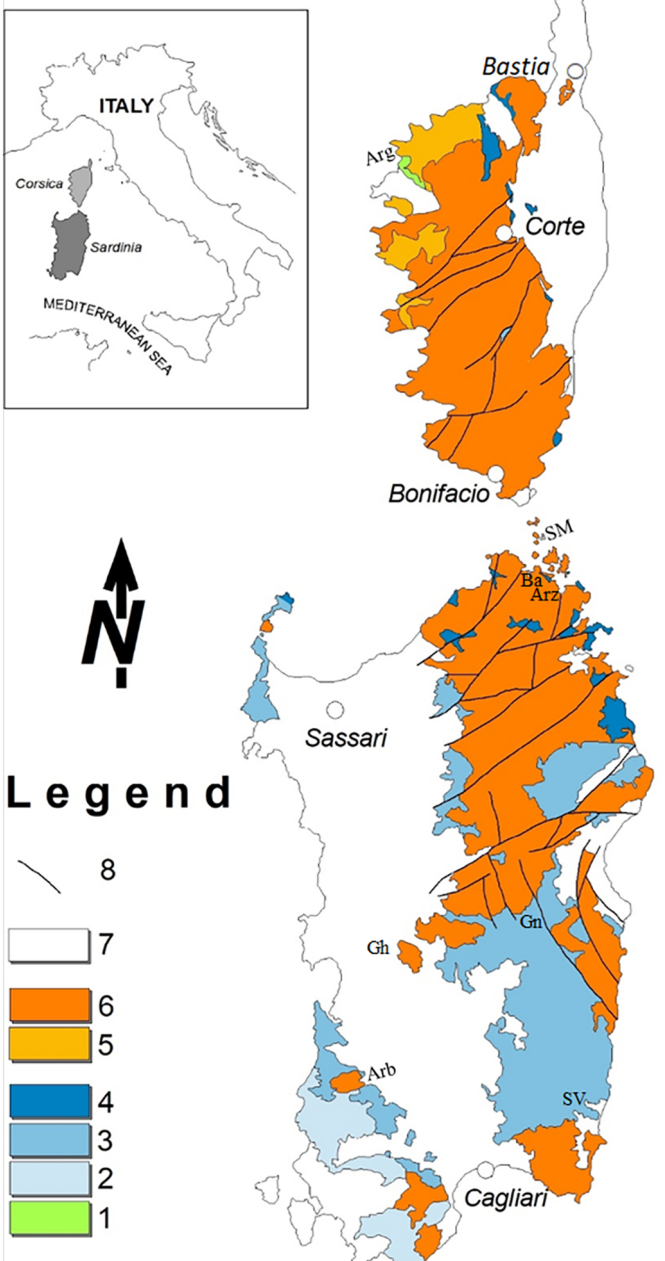
ITALY
Corsica
Sardinia
MEDITERRANEAN SEA
Bastia
Arg
Corte
Bonifacio
SM
Ba
Arz
Sassari
Gn
Gh
Arb
SV
Cagliari
Legend
8
7
6
5
4
3
2
1

Figure 1

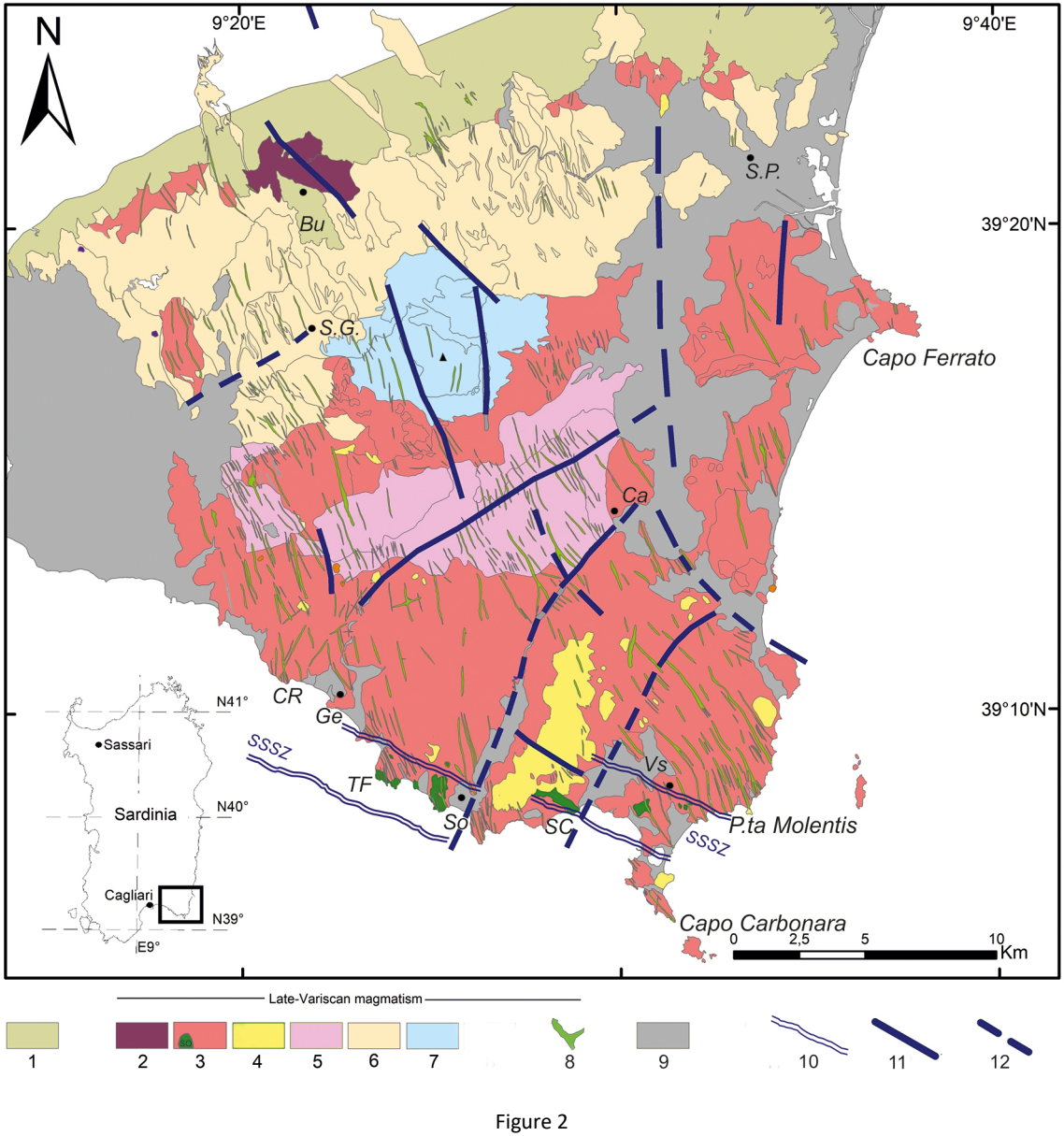
N
9°20'E
9°40'E
39°20'N
39°10'N
Bu
S.P.
S.G.
Capo Ferrato
Ca
CR
Ge
SSSZ
TF
So
SC
Vs
P.ta Molentis
SSSZ
Capo Carbonara
0
2,5
5
10
Km
N41°
Sassari
Sardinia
N40°
Cagliari
N39°
E9°
Late-Variscan magmatism
1
2
3
4
5
6
7
8
9
10
11
12

Figure 2

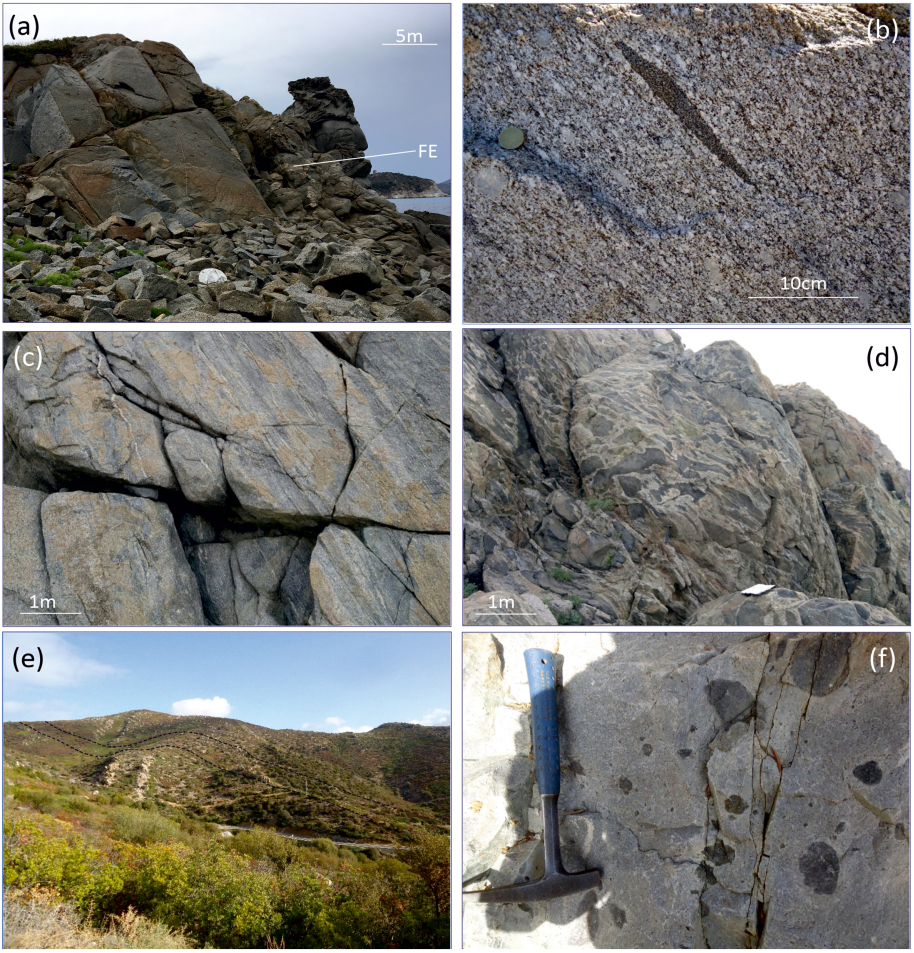

Figure 3

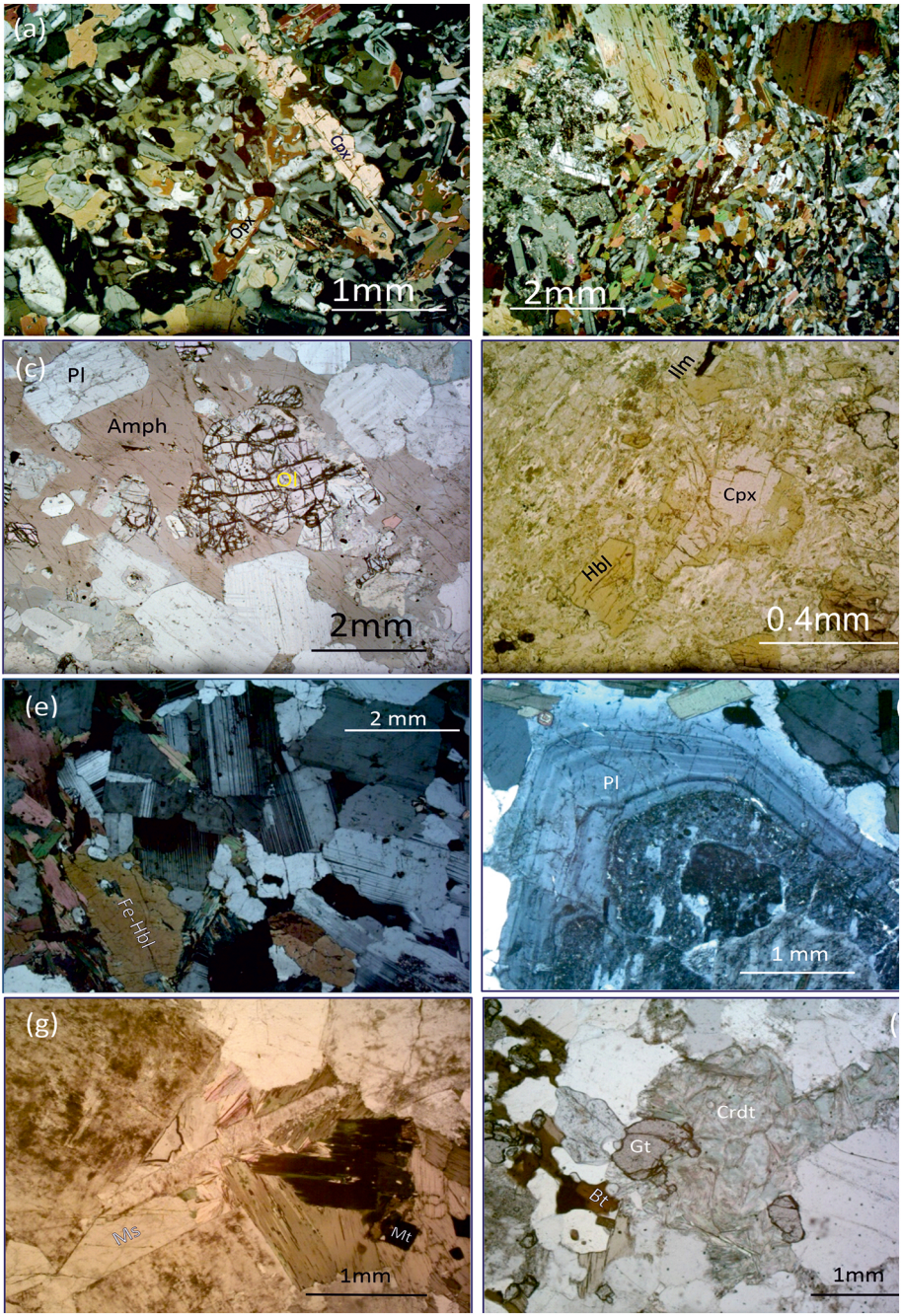
(a)
Cpx
Opx
1mm
2mm
(c)
Pl
Amph
2mm
Ilm
Cpx
Hbl
0.4mm
(e)
2 mm
Fe-Hbl
Pl
1 mm
(g)
Ms
Mt
1mm
Crdt
Gt
Bt
1mm

Figure 4

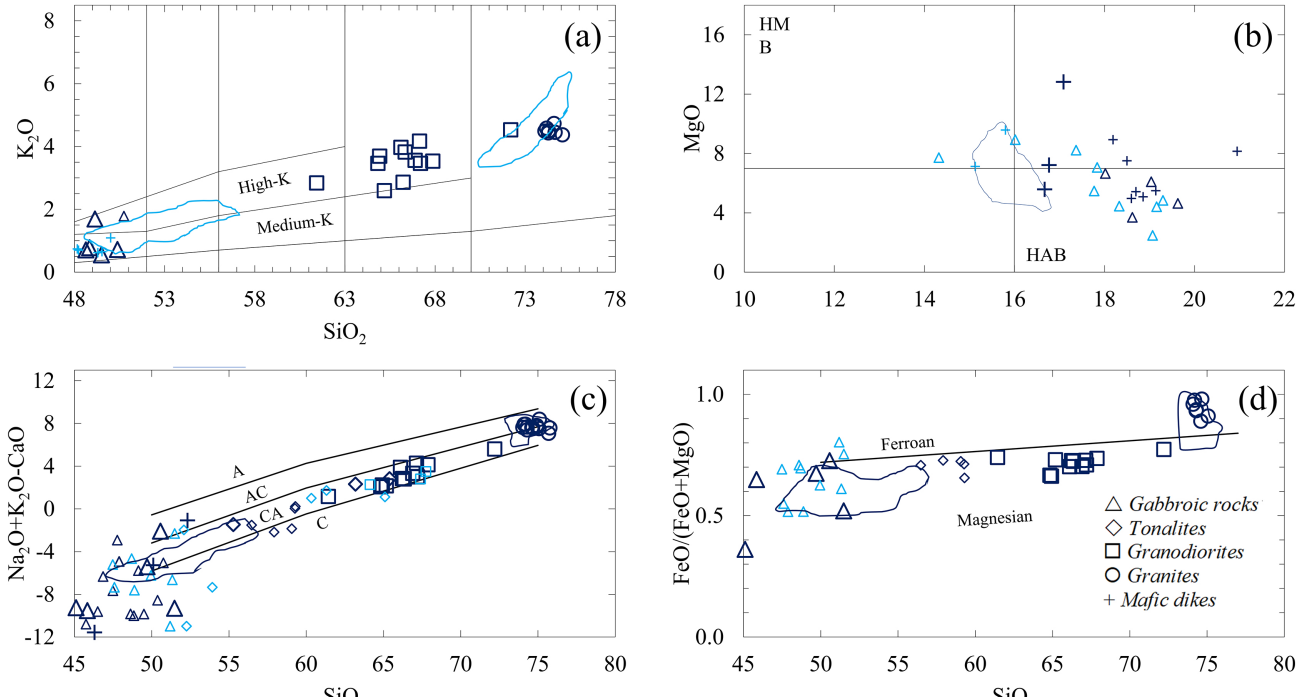
(a)
K_2O
SiO_2
High-K
Medium-K
(b)
HM
B
MgO
HAB
(c)
Na_2O+K_2O-CaO
SiO_2
A
AC
CA
C
(d)
FeO/(FeO+MgO)
SiO_2
Ferroan
Magnesian
Gabbroic rocks
Tonalites
Granodiorites
Granites
Mafic dikes

Figure 5

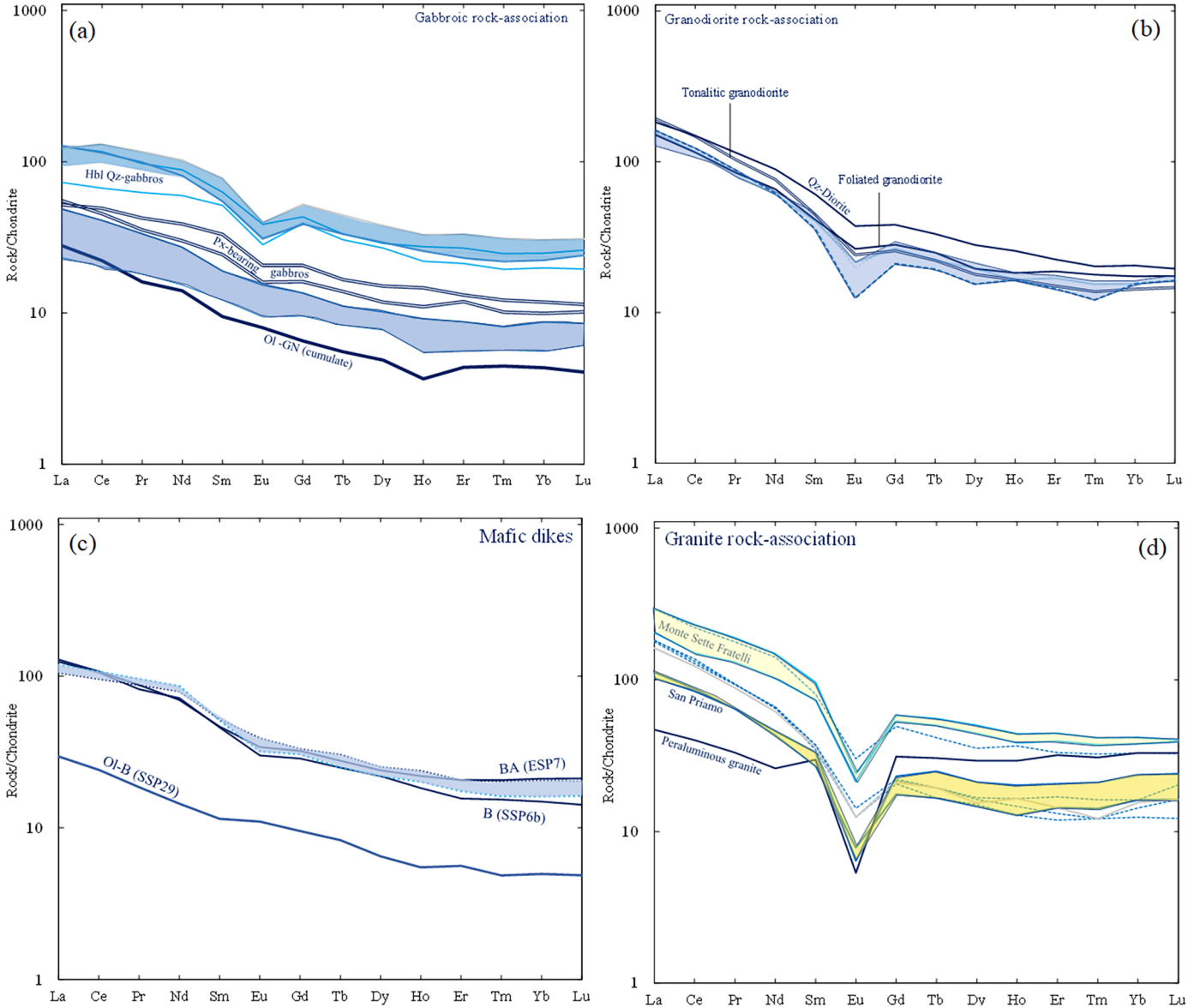
(a)
Gabbroic rock-association
Hbl Qz-gabbros
Px-bearing gabbros
Ol -GN (cumulate)
(b)
Granodiorite rock-association
Tonalitic granodiorite
Foliated granodiorite
Qz-Diorite
(c)
Mafic dikes
BA (ESP7)
B (SSP6b)
Ol-B (SSP29)
(d)
Granite rock-association
Monte Sette Fratelli
San Priamo
Peraluminous granite
Rock/Chondrite
1000
100
10
1
La Ce Pr Nd Sm Eu Gd Tb Dy Ho Er Tm Yb Lu

Figure 6

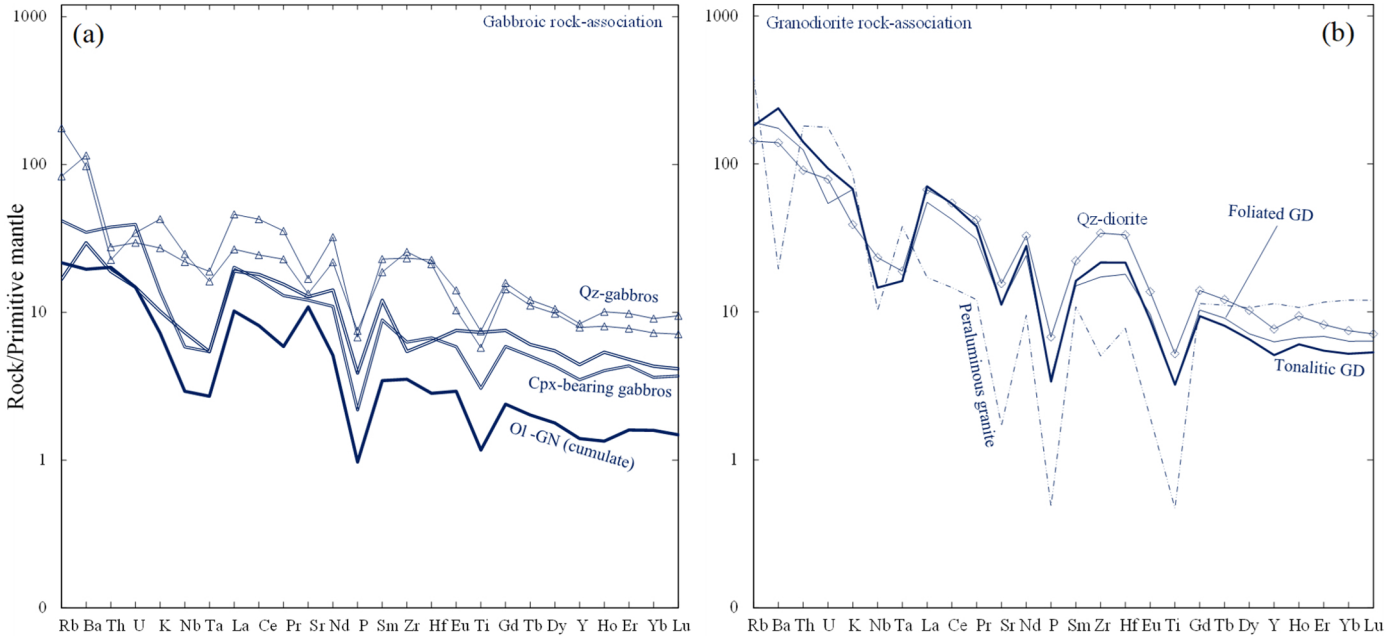
(a)
Gabbroic rock-association
Rock/Primitive mantle
1000
100
10
1
0
Qz-gabbros
Cpx-bearing gabbros
Ol -GN (cumulate)
Rb Ba Th U K Nb Ta La Ce Pr Sr Nd P Sm Zr Hf Eu Ti Gd Tb Dy Y Ho Er Yb Lu
(b)
Granodiorite rock-association
Qz-diorite
Foliated GD
Peraluminous granite
Tonalitic GD
Rb Ba Th U K Nb Ta La Ce Pr Sr Nd P Sm Zr Hf Eu Ti Gd Tb Dy Y Ho Er Yb Lu

Figure 7

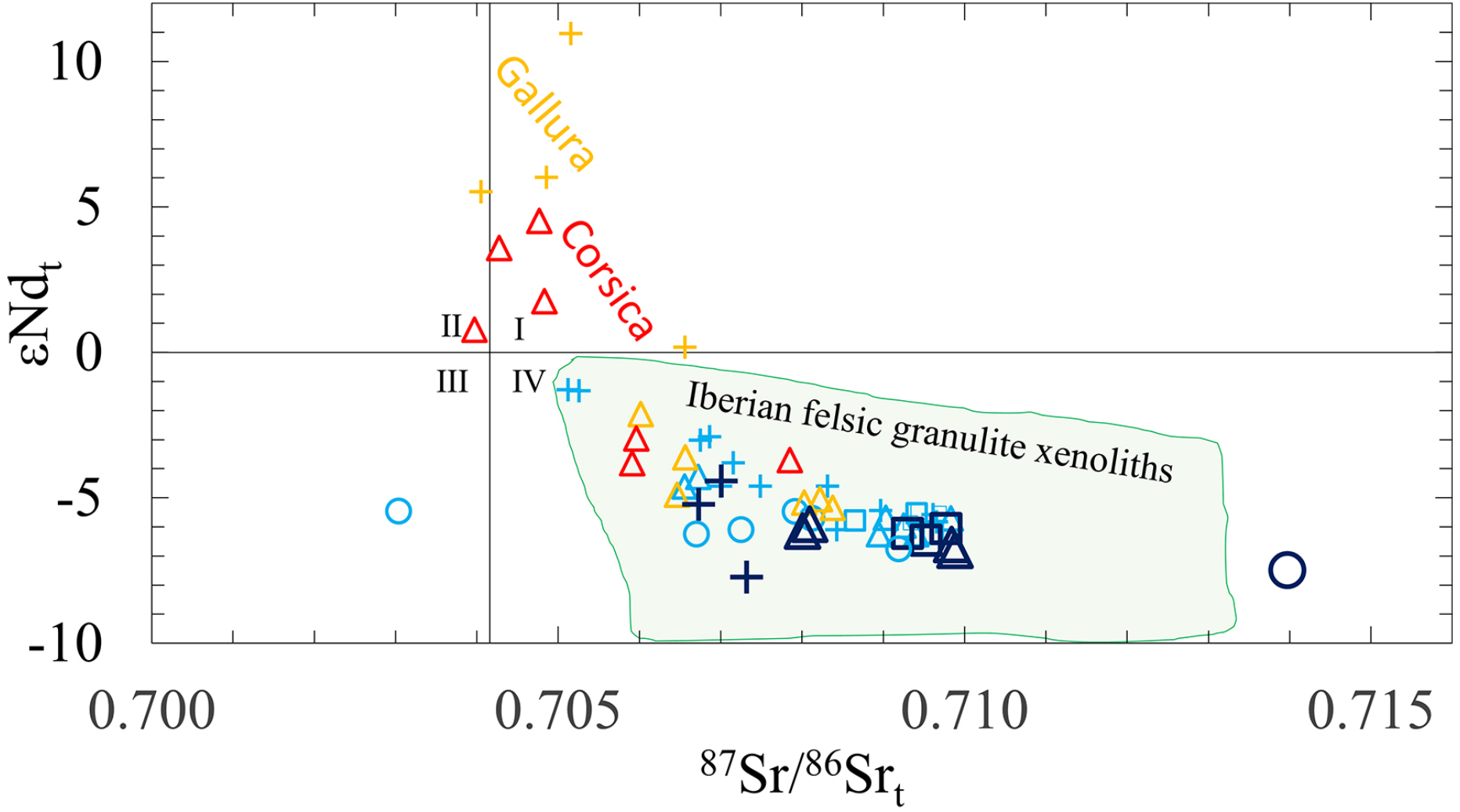
10
5
0
-5
-10
εNd$_t$
0.700
0.705
0.710
0.715
$^{87}Sr/^{86}Sr_t$
Gallura
Corsica
II
I
III
IV
Iberian felsic granulite xenoliths

Figure 8

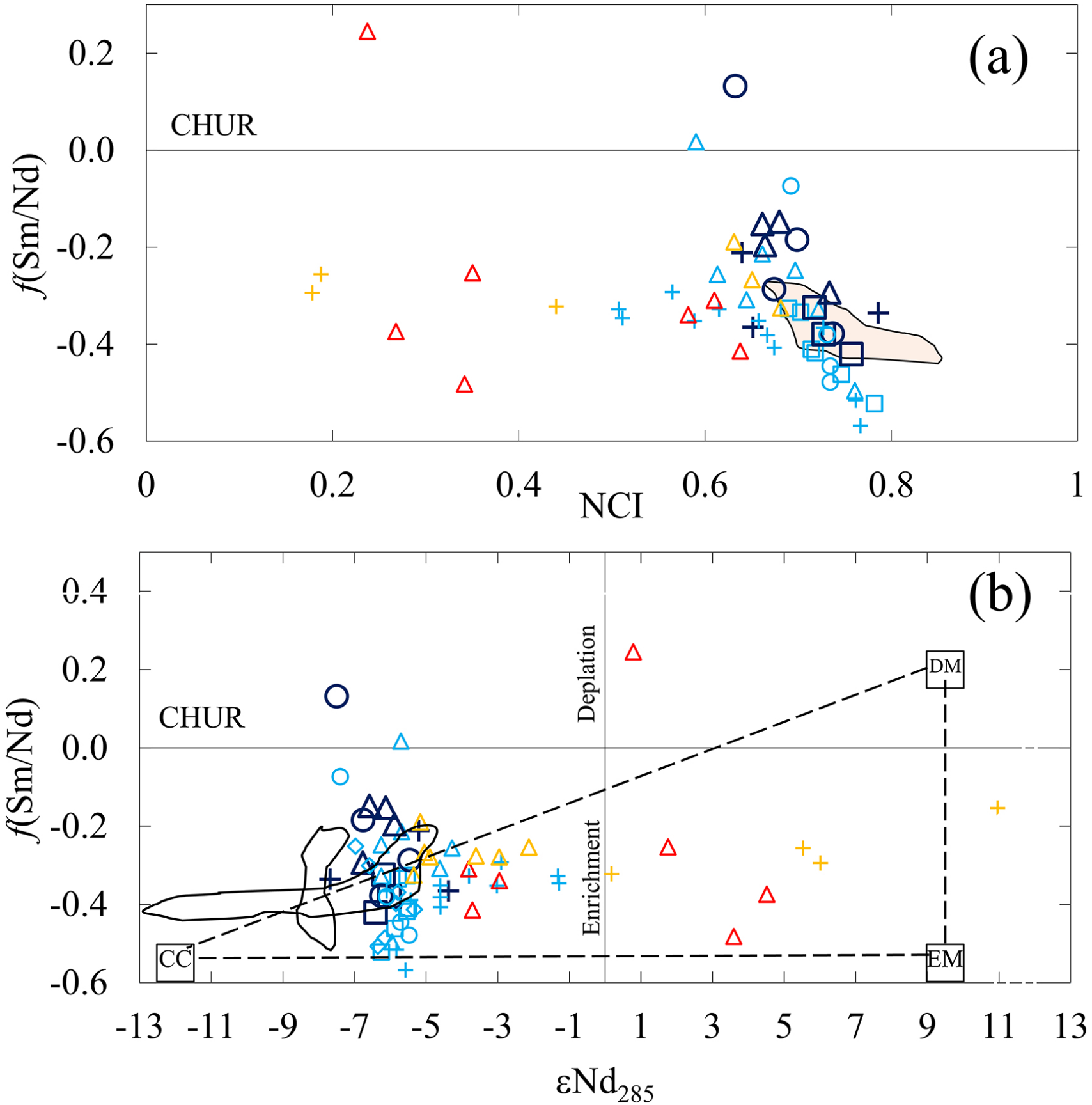
(a)
CHUR
f(Sm/Nd)
0.2
0.0
-0.2
-0.4
-0.6
0
0.2
0.4
0.6
0.8
1
NCI
(b)
CHUR
Deplation
Enrichment
DM
CC
EM
f(Sm/Nd)
0.4
0.2
0.0
-0.2
-0.4
-0.6
-13
-11
-9
-7
-5
-3
-1
1
3
5
7
9
11
13
εNd285

Figure 9

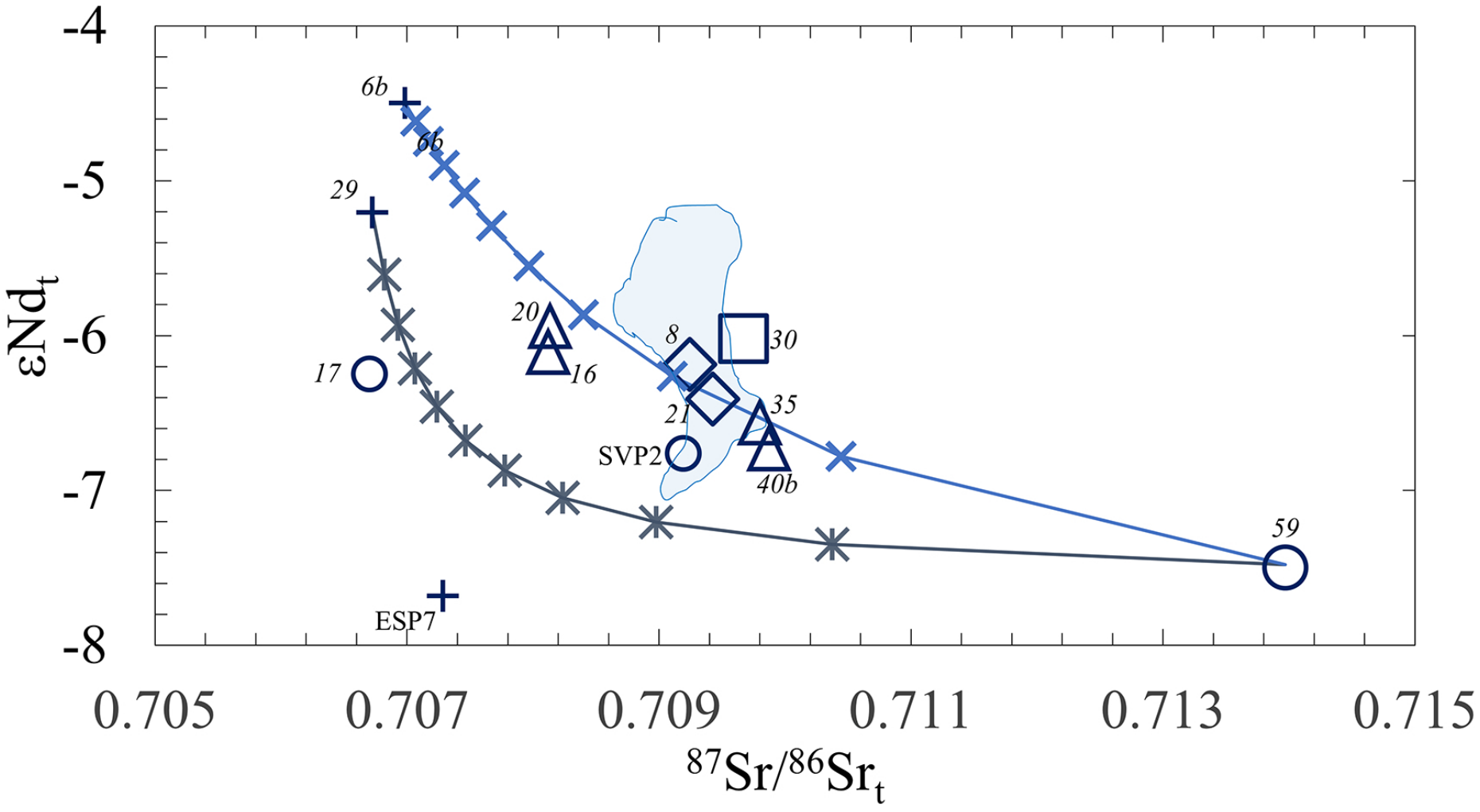
-4
-5
-6
-7
-8
εNd$_t$
0.705
0.707
0.709
0.711
0.713
0.715
$^{87}Sr/^{86}Sr_t$
6b
6b
29
20
16
17
8
30
21
35
SVP2
40b
59
ESP7

Figure 10